

A WTLS-Based Method for Remote Sensing Imagery Registration

Tianjun Wu, Yong Ge, *Member, IEEE*, Jianghao Wang, Alfred Stein, Yongze Song, Yunyan Du, and Jianghong Ma

Abstract—This paper introduces a weighted total least squares (WTLS)-based estimator into image registration to deal with the coordinates of control points (CPs) that are of unequal accuracy. The performance of the estimator is investigated by means of simulation experiments using different coordinate errors. Comparisons with ordinary least squares (LS), total LS (TLS), scaled TLS, and weighted LS estimators are made. A novel adaptive weight determination scheme is applied to experiments with remotely sensed images. These illustrate the practicability and effectiveness of the proposed registration method by collecting CPs with different-sized errors from multiple reference images with different spatial resolutions. This paper concludes that the WTLS-based iteratively reweighted TLS method achieves a more robust estimation of model parameters and higher registration accuracy if heteroscedastic errors occur in both the coordinates of reference CPs and target CPs.

Index Terms—Adaptive weight scheme, image registration, unequal accuracy, weighted total least squares (WTLS).

I. INTRODUCTION

ACCURATE registration of remotely sensed images is required in many applications such as land cover/use change detection and environmental monitoring. Two types of registration models are distinguished to do so, i.e., physical models and empirical models [1], [2]. Physical models, such as collinearity equations, can achieve high positioning accuracy based on a minimal number of pairs of control points (CPs), but they require a precise satellite ephemeris. Empirical models use statistical relations with parameters estimated on the basis of collected CPs. As the physical parameters and prior sensor

information cannot be accessed easily, empirical models are widely used, e.g., polynomial functions, rational functions, and splines. In particular, polynomial regression models are commonly applied in image registration.

In a polynomial regression model, the coordinates of reference CPs (RCPs, i.e., CPs extracted from reference images) used as explanatory variables are assumed to be error-free, whereas the errors in the coordinates of target CPs (TCPs, i.e., CPs extracted from distorted images) used as response variables are assumed to be independent and identically distributed. The coordinates of RCPs, however, are usually not free of errors as they are mainly obtained from geographic information systems and remotely sensed images [3], [4]. In this situation, the use of the ordinary least squares (LS) estimator will result into the biased estimation of the coefficients of the polynomials because errors in the RCP coordinates are ignored [4]. In [4], we introduced a consistent adjusted LS (CALS) estimator and proposed a relaxed CALS (RCALS) estimator to partly overcome such a problem.

Recently, the total LS (TLS) estimator [5]–[9] and the scaled TLS (STLS) estimator [10] have been devised on the basis of error-in-variables (EIV) modeling to handle the errors in the explanatory variable data. The assumptions in CALS and RCALS estimators are partly relaxed. Their basic concept is to estimate the parameters of the EIV model by minimizing the orthogonal distance from the measured data of the explanatory variable and the response variable to the fitted EIV model [5]–[11]. In [11], we introduced the STLS estimator to correct the errors contained in the RCPs. However, it is found that this method is inadequate when it works with real data. A homoscedastic error structure is required for the STLS estimator with the EIV model, which means that the variances of the errors in the data of the explanatory variable and of the response variable are equal [7], [10], [11]. In image registration, however, the CPs may have varying accuracy values. Their measured errors commonly have a nonidentical distribution. For instance, some RCPs are obtained from fine-scale maps and others from coarse-scale maps. Collecting RCPs from multiple reference images may lead to RCPs with different accuracy values. As the measurement errors in the data of the explanatory variable and the response variable are of different sizes, the homoscedasticity assumptions in the TLS and STLS estimators are violated by the real error statistics of RCPs. Therefore, estimations using the TLS and STLS methods are not reliable.

General robust methods have been successively proposed to handle heteroscedastic data [12]–[14]. For example, [14] proposed a novel robust estimation algorithm, i.e., the generalized projection-based M -estimator, which does not require the user to specify any scale parameters on the application of robust regression. To deal with heteroscedastic data in the EIV

Manuscript received October 5, 2013; revised February 12, 2014; accepted March 31, 2014. Date of publication May 29, 2014; date of current version August 4, 2014. This work was supported in part by the Knowledge Innovation Program of the Chinese Academy of Sciences (Grant KZCX2-EW-QN303), the Innovation Program of the Institute of Geographic Sciences & Natural Resources Research (Grant 201003009) and the National Marine Public Welfare Research Project of China (201105033). (*Corresponding author: Yong Ge.*)

T. Wu is with the State Key Laboratory of Remote Sensing Sciences, Institute of Remote Sensing and Digital Earth (RADI), Chinese Academy of Sciences, Beijing 100101, China (e-mail: tjwucn@gmail.com).

Y. Ge, J. Wang, and Y. Du are with the State Key Laboratory of Resource and Environmental Information System, Institute of Geographical Sciences and Natural Resources Research, Chinese Academy of Sciences, Beijing 100101, China (e-mail: gey@lreis.ac.cn).

A. Stein is with the Faculty of Geo-Information Science and Earth Observation (ITC), University of Twente, 7514 AE Enschede, The Netherlands (e-mail: a.stein@utwente.nl).

Y. Song is with the China University of Geosciences, Beijing 100083, China, and also with the Institute of Geographic Sciences and Natural Resources Research, Chinese Academy of Sciences, Beijing 100101, China (e-mail: eterne2@163.com).

J. Ma is with the Department of Mathematics and Information Science, Chang'an University, Xi'an 710064, China (e-mail: jhma@chd.edu.cn).

Digital Object Identifier 10.1109/TGRS.2014.2318705

model, the weighted TLS (WTLS) estimator was proposed by Markovsky *et al.* [15]. In this approach, the different accuracy values of the explanatory variable and the response variable are taken into account, and their error structures are relaxed into a more general relationship. Estimation by this method can be then done by minimizing the weighted orthogonal distance [16]. In this way, the WTLS estimator unifies the LS, weighted LS (WLS) [17], TLS, and STLS estimators, and is thus more realistic in practical applications. As an application-oriented method, this estimator has been recently used in various applications [18]–[21].

The EIV-model-based WTLS method is suited to situations in which the CPs from remotely sensed imagery are corrupted by noise with nonidentical probability distributions. Hence, this paper introduces a WTLS-based iteratively reweighted TLS (IRTLS) method into remotely sensed imagery registration. The novelty of the proposed methodology with regard to previously developed methods [1], [2] is that it can jointly take the different-sized errors in the RCPs and TCPs into account. The effect of low-accuracy and high-accuracy CPs on registration can be distinguished by the weights in the estimator. Furthermore, to guarantee its practicability, a two-sided adaptively weighting scheme is derived to determine the weights of RCPs and TCPs during registration. In this way, the limitations of conventional estimators can be overcome, and the robustness and accuracy of remotely sensed imagery registration is potentially improved. To show its performance, this paper is illustrated with a simulation experiment and two experiments on different types of remote sensing images. During these experiments, the performance of our IRTLS method is compared with the common LS, TLS, STLS, and WLS estimators.

II. WTLS ESTIMATOR FOR IMAGE REGISTRATION

The focus of this paper is the measurement errors in RCPs and TCPs. Let the observed coordinates of an RCP in the reference image be denoted by $g = (g_x, g_y)$, and let the observed coordinate of a TCP in the distorted image be denoted by $u = (u_x, u_y)$. A second-order polynomial regression model to explain the true coordinates on the basis of RCPs can be represented by [22]–[25]

$$u = v^T \boldsymbol{\beta} + \varepsilon \quad (1)$$

where $\boldsymbol{\beta} = (\boldsymbol{\beta}_x, \boldsymbol{\beta}_y)$, $\boldsymbol{\beta}_x = (\beta_{x0}, \beta_{x1}, \beta_{x2}, \beta_{x3}, \beta_{x4}, \beta_{x5})^T$, and $\boldsymbol{\beta}_y = (\beta_{y0}, \beta_{y1}, \beta_{y2}, \beta_{y3}, \beta_{y4}, \beta_{y5})^T$ are the unknown model coefficients; $v = (1, g_x, g_y, g_x g_y, g_x^2, g_y^2)^T$; and $\varepsilon = (\varepsilon_x, \varepsilon_y)$ is the measurement error of the TCP.

For the observed coordinates of RCPs containing measurement errors, the EIV model is introduced to the image registration [4], [11]. For a second-order linear EIV registration model, the unobserved “true” coordinates $U = (U_x, U_y)$ and $G = (G_x, G_y)$ of a TCP and an RCP are related by the following model:

$$U = V^T \boldsymbol{\beta} \quad (2)$$

where $V = (1, G_x, G_y, G_x G_y, G_x^2, G_y^2)^T$. Because of measurement errors $\varepsilon = (\varepsilon_x, \varepsilon_y)$ and $\delta = (\delta_x, \delta_y)$, we can only observe $u = (u_x, u_y)$ and $g = (g_x, g_y)$, i.e.,

$$\begin{cases} u = U + \mu \\ v = V + \varsigma \end{cases} \quad (3)$$

Here, $\varsigma = (0, \delta_x, \delta_y, \delta_x g_y + \delta_y g_x + \delta_x \delta_y, 2\delta_x g_x + \delta_x^2, 2\delta_y g_y + \delta_y^2)^T \sim (\mathbf{0}, \boldsymbol{\Sigma}_\varsigma) = (\mathbf{0}, \sigma_0^2 \mathbf{P}_\varsigma)$, $\mu \equiv \varepsilon = (\varepsilon_x, \varepsilon_y) \sim (\mathbf{0}, \boldsymbol{\Sigma}_\mu) = (\mathbf{0}, \sigma_0^2 \mathbf{P}_\mu)$, where $\boldsymbol{\Sigma}_\varsigma$ and $\boldsymbol{\Sigma}_\mu$ are the covariance matrices of the errors of CPs, σ_0^2 is a variance scalar factor, and \mathbf{P}_ς and \mathbf{P}_μ are the cofactor matrices. Thus, for n pairs of independently collected CPs, we write

$$\begin{aligned} \mathbf{U} &\equiv \begin{bmatrix} U_1 \\ \vdots \\ U_n \end{bmatrix} & \mathbf{V} &\equiv \begin{bmatrix} V_1^T \\ \vdots \\ V_n^T \end{bmatrix} & \mathbf{g} &\equiv \begin{bmatrix} g_1 \\ \vdots \\ g_n \end{bmatrix} \\ \mathbf{u} &\equiv \begin{bmatrix} u_1 \\ \vdots \\ u_n \end{bmatrix} & \mathbf{v} &\equiv \begin{bmatrix} v_1^T \\ \vdots \\ v_n^T \end{bmatrix} & \boldsymbol{\mu} &\equiv \begin{bmatrix} \mu_1 \\ \vdots \\ \mu_n \end{bmatrix} & \boldsymbol{\varsigma} &\equiv \begin{bmatrix} \varsigma_1^T \\ \vdots \\ \varsigma_n^T \end{bmatrix} \\ \boldsymbol{\Sigma}_\mu &\equiv \text{diag}([\boldsymbol{\Sigma}_{\mu_1}, \boldsymbol{\Sigma}_{\mu_2}, \dots, \boldsymbol{\Sigma}_{\mu_n}]) = \sigma_0^2 \mathbf{P}_\mu \\ \mathbf{P}_\mu &\equiv \text{diag}([\mathbf{P}_{\mu_1}, \mathbf{P}_{\mu_2}, \dots, \mathbf{P}_{\mu_n}]) \\ \boldsymbol{\Sigma}_\varsigma &\equiv \text{diag}([\boldsymbol{\Sigma}_{\varsigma_1}, \boldsymbol{\Sigma}_{\varsigma_2}, \dots, \boldsymbol{\Sigma}_{\varsigma_n}]) = \sigma_0^2 \mathbf{P}_\varsigma \\ \mathbf{P}_\varsigma &\equiv \text{diag}([\mathbf{P}_{\varsigma_1}, \mathbf{P}_{\varsigma_2}, \dots, \mathbf{P}_{\varsigma_n}]) \end{aligned}$$

where $\text{diag}(\cdot)$ is a diagonal matrix whose diagonal elements are contained in a vector. Then, the matrix form of the linear EIV registration model can be written as

$$\begin{cases} \mathbf{U} = \mathbf{V}\boldsymbol{\beta} \\ \mathbf{u} = \mathbf{U} + \boldsymbol{\mu} \\ \mathbf{v} = \mathbf{V} + \boldsymbol{\varsigma} \end{cases} \quad (4)$$

Let the properties of errors be characterized by

$$\begin{bmatrix} \text{vec}(\boldsymbol{\mu}) \\ \text{vec}(\boldsymbol{\varsigma}) \end{bmatrix} \sim \left(\begin{bmatrix} \mathbf{0} \\ \mathbf{0} \end{bmatrix}, \begin{bmatrix} \boldsymbol{\Sigma}_\mu & \\ & \boldsymbol{\Sigma}_\varsigma \end{bmatrix} \right) = \left(\begin{bmatrix} \mathbf{0} \\ \mathbf{0} \end{bmatrix}, \sigma_0^2 \begin{bmatrix} \mathbf{P}_\mu & \\ & \mathbf{P}_\varsigma \end{bmatrix} \right) \quad (5)$$

where $\text{vec}(\cdot)$ denotes the columnwise vectorization of a matrix [26]. In this model, cofactor matrices \mathbf{P}_μ and \mathbf{P}_ς can be expressed as $\mathbf{P}_\mu = \mathbf{P}_{0,\mu} \otimes \mathbf{P}_\varepsilon$ and $\mathbf{P}_\varsigma = \mathbf{P}_{0,\varsigma} \otimes \mathbf{P}_\delta$, respectively, where $\mathbf{P}_{0,\mu}$ and $\mathbf{P}_{0,\varsigma}$ are matrices that are proportional to diagonal matrices whose diagonal elements are the variances of each dimension in explanatory variable v and response variable u , respectively; \otimes is the Kronecker product; and $\mathbf{P}_\varepsilon = \text{diag}([p_{\varepsilon_1}, p_{\varepsilon_2}, \dots, p_{\varepsilon_n}])$ and $\mathbf{P}_\delta = \text{diag}([p_{\delta_1}, p_{\delta_2}, \dots, p_{\delta_n}])$ are the cofactor matrices of covariance matrices $\boldsymbol{\Sigma}_\varepsilon = \sigma_0^2 \mathbf{P}_\varepsilon = \text{diag}([\sigma_{\varepsilon_1}^2, \sigma_{\varepsilon_2}^2, \dots, \sigma_{\varepsilon_n}^2])$ and $\boldsymbol{\Sigma}_\delta = \sigma_0^2 \mathbf{P}_\delta = \text{diag}([\sigma_{\delta_1}^2, \sigma_{\delta_2}^2, \dots, \sigma_{\delta_n}^2])$, respectively. According to the polynomial structure and variance-covariance propagation law [22], we have $\mathbf{P}_{0,\mu} \propto \text{diag}([\sigma_{\delta_x}^2, \sigma_{\delta_y}^2])$ and $\mathbf{P}_{0,\varsigma} \propto \text{diag}([0, \sigma_{\delta_x}^2, \sigma_{\delta_y}^2, g_x^2 \sigma_{\delta_y}^2 + g_y^2 \sigma_{\delta_x}^2, 4g_x^2 \sigma_{\delta_x}^2, 4g_y^2 \sigma_{\delta_y}^2])$. Therefore, we set $\mathbf{P}_{0,\varsigma} \approx \text{diag}([0, 1, 1, \text{mean}(\mathbf{g}_x^2 + \mathbf{g}_y^2), \text{mean}(4\mathbf{g}_x^2), \text{mean}(4\mathbf{g}_y^2)])$ and $\mathbf{P}_{0,\mu} \approx \text{diag}([1, 1])$ as approximations, where $\text{mean}(\cdot)$ denotes the mean value of a vector, $\mathbf{g}_x = (g_{x1}, g_{x2}, \dots, g_{xn})^T$, and $\mathbf{g}_y = (g_{y1}, g_{y2}, \dots, g_{yn})^T$.

The linear EIV model (4) is equivalent to the polynomial regression model if $\boldsymbol{\Sigma}_\varsigma = \mathbf{0}$ [27]–[30]. In the homoscedastic case of (4), it is assumed that $\mathbf{P}_\varepsilon = \mathbf{I}$ and that $\mathbf{P}_\delta = \mathbf{I}$. Under these assumptions, the EIV-based TLS [5]–[9] and STLS estimators [10], [11] can provide consistent estimations of the unknown parameters, i.e., the estimations converge to the true values as the number of samples tends to infinity. The LS estimator, however, is inconsistent and asymptotically biased if errors exist in both the response and explanatory variables. In the registration, the size of measurement errors δ in the coordinates of RCPs g used as an explanatory variable may differ owing to human errors, instrumental errors, and other reasons. Additionally, the error ε in the coordinates of response

variable u may also vary owing to observation errors. Therefore, the assumptions underlying the use of the TLS and STLS estimators are violated.

To deal with these problems of varying accuracy values, the WTLS estimator was introduced by Markovsky *et al.* [15]. This estimator assumes that the error structure differs at each data point, irrespective of response variable u or explanatory variable g . Their relative sizes are determined by covariance matrices Σ_ε and Σ_δ . That is, cofactor matrices \mathbf{P}_ε and \mathbf{P}_δ are used to characterize the accuracy of the data for both explanatory variable g and response variable u . The optimal weight matrices for this estimator are defined as

$$\begin{cases} \mathbf{W}_\varepsilon = \mathbf{P}_\varepsilon^{-1} = \sigma_0^2 \Sigma_\varepsilon^{-1} = \text{diag}([w_{\varepsilon_1}, w_{\varepsilon_2}, \dots, w_{\varepsilon_n}]) \\ \mathbf{W}_\delta = \mathbf{P}_\delta^{-1} = \sigma_0^2 \Sigma_\delta^{-1} = \text{diag}([w_{\delta_1}, w_{\delta_2}, \dots, w_{\delta_n}]) \end{cases} \quad (6)$$

where $w_{\varepsilon_i} = \sigma_0^2 / \sigma_{\varepsilon_i}^2$, $w_{\delta_i} = \sigma_0^2 / \sigma_{\delta_i}^2$, $i = 1, \dots, n$. Then, with the pairs of coordinates $[\mathbf{u}, \mathbf{g}]$ and weight matrices \mathbf{W}_ε and \mathbf{W}_δ , the objective of the WTLS estimator is written as

$$\begin{aligned} \min_{\hat{\beta}_{\text{WTLS}}} Q_{\text{WTLS}}(\hat{\beta}_{\text{WTLS}}) \\ = \text{vec}(\boldsymbol{\mu})^T \mathbf{W}_\mu^{-1} \text{vec}(\boldsymbol{\mu}) + \text{vec}(\boldsymbol{\varsigma})^T \mathbf{W}_\varsigma^{-1} \text{vec}(\boldsymbol{\varsigma}) \end{aligned} \quad (7)$$

where $\mathbf{W}_\mu = \mathbf{W}_{0,\mu} \otimes \mathbf{W}_\varepsilon$, $\mathbf{W}_\varsigma = \mathbf{W}_{0,\varsigma} \otimes \mathbf{W}_\delta$, $\mathbf{W}_{0,\mu} = \mathbf{P}_{0,\mu}^{-1}$, and $\mathbf{W}_{0,\varsigma} = \mathbf{P}_{0,\varsigma}^{-1}$. Once the minimal $Q_{\text{WTLS}}(\hat{\beta}_{\text{WTLS}})$ is found, its solution $\hat{\beta}_{\text{WTLS}} = (\hat{\beta}_{x,\text{WTLS}}, \hat{\beta}_{y,\text{WTLS}})$ is called the WTLS solution of the EIV model [15].

Unlike the LS and WLS estimators, the WTLS estimator has no analytic closed-form solution in the general case, and numerical iterative optimization methods are therefore employed to find the solution. This problem is discussed in more detail in [15], and [31]–[33]. To guarantee convergence to the global solution, the solution in this paper is solved using the iterative algorithm in [32]. For a comprehensive introduction to the WTLS theory, algorithms, and some of its applications, we refer to the work in [31].

III. EXPERIMENTS WITH SIMULATION IMAGES

In the remainder of this paper, we apply the WTLS estimator to improve the accuracy and robustness of image registration. Using images and errors with simple but well-defined properties is helpful to better understand the characteristics and effects of the proposed methodology on the improvement of the registration. Therefore, a simulation experiment is designed to investigate the performance of the WTLS method. This adjustable experiment environment is convenient to control the model parameters and the environment settings.

A. Design of Simulation Experiments

1) *Preparation of Images for Experiments:* A 1200×1200 -pixel thematic raster map with three classes in equal proportions is simulated as the reference image. The pixel values of the three classes are set at 0, 51, and 128, respectively, as shown in Fig. 1. The spatial resolutions of the three bands are assumed to be $\text{SR}_{\text{ref}} = 1$ m.

The corresponding distorted image is artificially generated from the reference image by resampling, introducing a system distortion, and introducing random location errors [11]. As shown in Fig. 2(a), the resampled reference image of $400 \times$

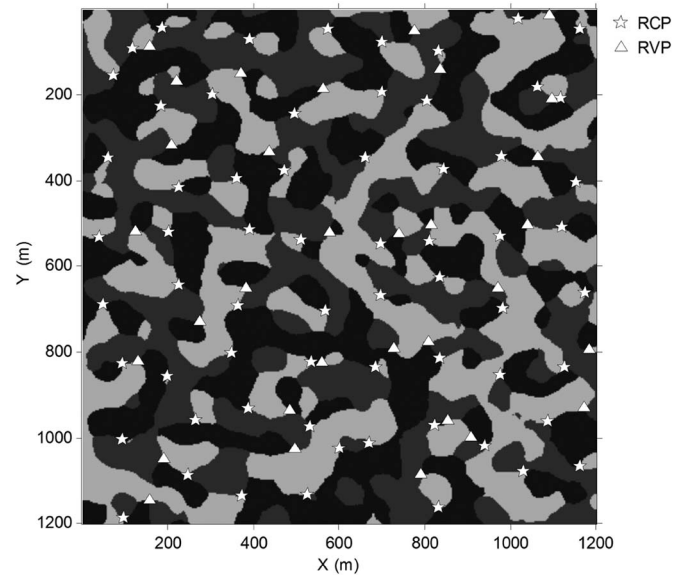


Fig. 1. Simulated reference image and the arrangement of RCPs and RVPs.

400 pixels and $\text{SR}_{\text{cor}} = 3$ m spatial resolution is resampled from Fig. 1. Fig. 2(b) shows the deterministic warping result obtained by applying the quadratic polynomial transformations with coefficient vectors $\beta_x = (50, 0.99, -0.1, 3e-5, 3e-5, -3e-5)^T$ and $\beta_y = (50, 0.1, 0.99, 3e-5, -3e-5, 3e-5)^T$. Other distortions could be also applied to introduce a system distortion in this simulation, such as affine transformations or perspective transformations [34]. After obtaining Fig. 2(b), random location errors are introduced to the coordinates of each point in the images. The scheme for adding errors will be detailed in the following section. Finally, resampling is used to reconstruct the new image with a random error distortion as the distorted image. We refer to [11] for further details of the artificially generated images.

2) *Adding Errors in CPs and Determining Weights:* The RCPs with coordinates $G = (G_x, G_y)$ evenly obtained from a reference image are taken as error-free RCPs, as shown in Fig. 1. To test the ability of the WTLS estimators to rectify deviation, we add random errors to the RCPs according to the following scheme:

$$\begin{cases} g_x = G_x + \delta_x = G_x + \sigma_{\delta_x} \times \text{rn} \times \text{SR}_{\text{ref}} \\ g_y = G_y + \delta_y = G_y + \sigma_{\delta_y} \times \text{rn} \times \text{SR}_{\text{ref}} \end{cases} \quad (8)$$

where rn denotes a random number generated from the standard normal distribution $N(0, 1)$. Thus, the errors of the RCPs in the x and y directions conform to normal distributions $N(0, \sigma_{\delta_x}^2)$ and $N(0, \sigma_{\delta_y}^2)$, respectively. The standard deviations in each direction σ_{δ_x} and σ_{δ_y} are determined by σ_δ and θ_δ , respectively, i.e.,

$$\begin{cases} \sigma_{\delta_x} = \sigma_\delta \times \cos(\theta_\delta) \\ \sigma_{\delta_y} = \sigma_\delta \times \sin(\theta_\delta) \end{cases} \quad (9)$$

where σ_δ and θ_δ are generated using the uniform random number ru at interval $[0, 1]$, i.e.,

$$\begin{cases} \sigma_\delta = \sigma_{\delta,\text{max}} \times \text{ru} \sim U[0, \sigma_{\delta,\text{max}}] \\ \theta_\delta = 2\pi \times \text{ru} \sim U[0, 2\pi]. \end{cases} \quad (10)$$

In (10), $U[a, b]$ denotes the uniform distribution of interval $[a, b]$. The randomly varying angle parameter θ_δ guarantees

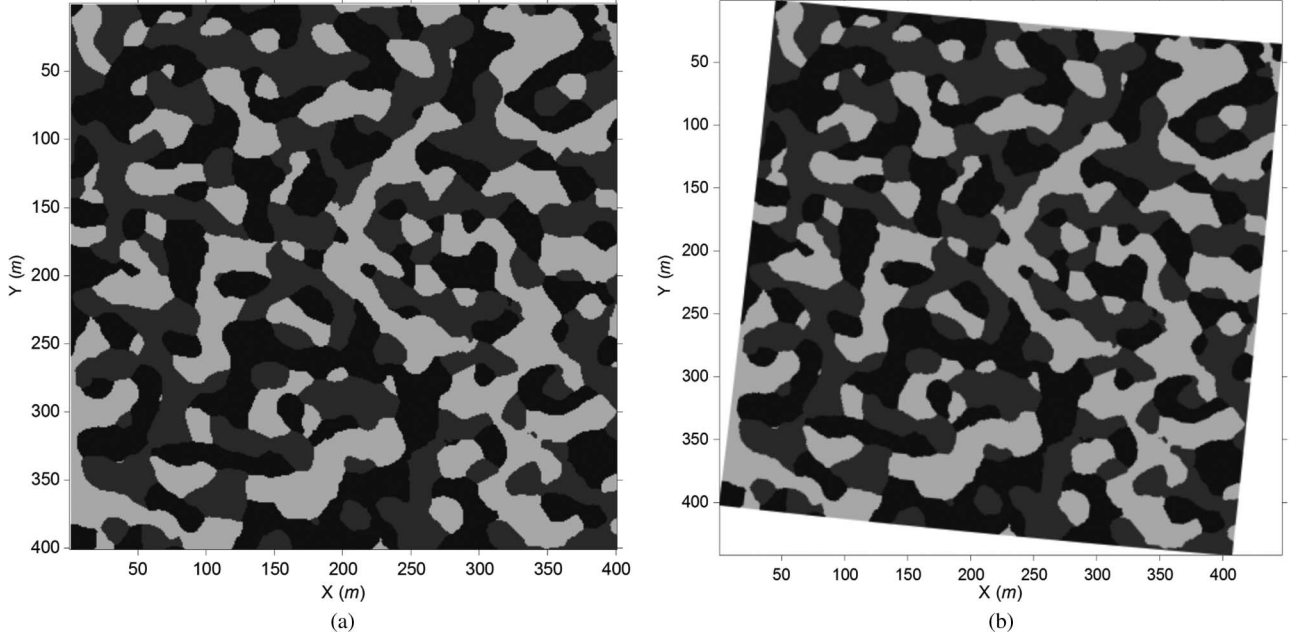


Fig. 2. Resampled reference image and distorted image. (a) Resampled reference image. (b) System-distorted image.

TABLE I
ONE REALIZATION OF SIMULATED DATA OF THE CPS AND VPS (UNIT: METERS)

Explanatory variable	Observed data		True data		Error		Standard deviation			Weight
	g_x	g_y	G_x	G_y	δ_x	δ_y	σ_{δ_x}	σ_{δ_y}	σ_{δ}	w_{δ}
RCP1	117.7774	92.6542	118.0000	93.0000	-0.2226	-0.3458	0.0853	0.1774	0.1969	0.0313
RCP2	187.9975	42.9502	188.0000	43.0000	-0.0025	-0.0498	0.0148	0.0298	0.0333	0.1851
.....
RVP1	159.2670	84.9890	159.0000	85.0000	0.2670	-0.0110	0.2014	0.0605	0.2103	0.1213
RVP2	219.9735	165.9988	220.0000	166.0000	-0.0265	-0.0012	0.0610	0.0024	0.0610	0.4181
.....
Response variable	Observed data		True data		Error		Standard deviation			Weight
	u_x	u_y	U_x	U_y	ε_x	ε_y	σ_{ε_x}	σ_{ε_y}	σ_{ε}	w_{ε}
TCP1	157.2529	154.1971	158.0075	154.0410	-0.7546	0.1561	1.0944	0.1830	1.1096	0.0020
TCP2	233.0576	110.6077	233.0674	110.6077	-0.0100	-0.0001	0.0216	0.0038	0.0219	0.1004
.....
TVP1	119.4082	149.8522	199.8571	149.9138	-0.4489	-0.0616	0.4949	0.0790	0.5012	0.2013
TVP2	253.0973	236.6530	252.9209	236.8103	0.1764	-0.1572	1.1124	0.6413	1.2840	0.0786
.....

that the directions of errors are random, whereas the maximal standard deviation of $\sigma_{\delta, \max} = 0.5$ pixel limits the errors at points $G = (G_x, G_y)$. Similarly, using a maximal standard deviation $\sigma_{\varepsilon, \max} = 1$ pixel, we can implement the addition of random errors in the error-free TCPs $U = (U_x, U_y)$ and obtain the error-added TCPs $u = (u_x, u_y)$.

According to the optimal weights in the WTLS estimator, the weights of the error-added pairs of CPs $u = (u_x, u_y)$ and $g = (g_x, g_y)$ are calculated, respectively, as

$$\begin{cases} w_{\varepsilon} = [\sigma_0^2 / \sigma_{\varepsilon}^2]_{\text{normalized}} \\ w_{\delta} = [\sigma_0^2 / \sigma_{\delta}^2]_{\text{normalized}} \end{cases} \quad (11)$$

where the variance scalar equals $\sigma_0^2 = 1$ in our study. Table I presents two examples of CPs and validation points (VPs, i.e., the points are not involved in the estimation process and are used to verify the outcomes of estimations) in one realization using the spatial relationship of the data, including the observed (i.e., error-added) data, the true (i.e., error-free) data, the errors, the standard deviations, and the normalized weights of the ex-

planatory and response variables. This example illustrates how to create simulated x and y coordinates and how to determine weights with the artificial added random errors.

3) *Model Estimation and Image Registration:* After collecting the pairs of points \mathbf{u} and \mathbf{g} , we centralize these error-added data and their corresponding weights $\mathbf{W}_{\varepsilon} = \text{diag}([w_{\varepsilon_1}, w_{\varepsilon_2}, \dots, w_{\varepsilon_n}])$ and $\mathbf{W}_{\delta} = \text{diag}([w_{\delta_1}, w_{\delta_1}, \dots, w_{\delta_1}])$, and then, we enter them into the EIV registration model to estimate model coefficients $\hat{\beta} = (\hat{\beta}_x, \hat{\beta}_y)$. Performances are compared after model estimation, and the corresponding registered images can be obtained by employing correcting technologies.

4) *Accuracy Assessment:* In the experiment, two aspects of assessments are adopted to quantitatively evaluate the performances of registration, i.e., coefficient estimation and registration errors.

a) *Coefficient estimations:* We compare coefficient estimates $\hat{\beta}$ in terms of their variance, bias, and MSE. These quantities can, respectively, assess the precision, accuracy, and robustness of the estimations [11].

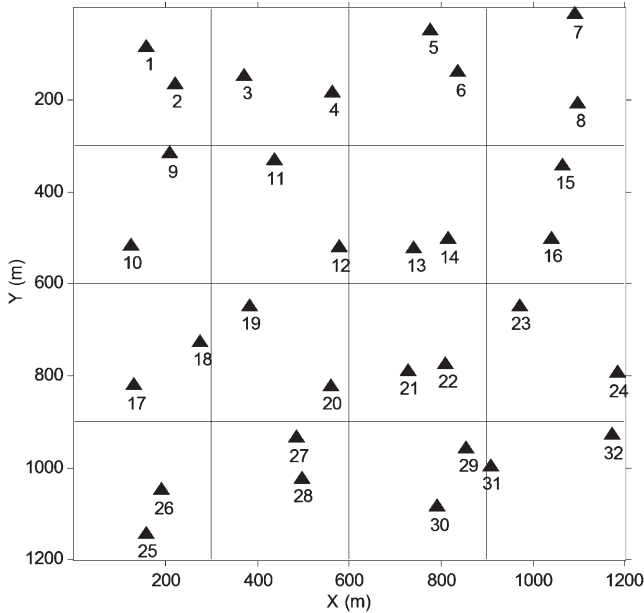


Fig. 3. Distribution of RVPs in the simulation experiment.

b) Registration errors: In addition to directly comparing the coefficient estimation, the root MSE (RMSE) metric of the VPs is commonly used during image registration. Fig. 3 shows a distribution of 32 VPs with a stratified simple random sampling. The errors in both the x and y directions $\hat{\delta} = (\hat{\delta}_x, \hat{\delta}_y)$ at these VPs are used to calculate the RMSE as follows:

$$\text{RMSE} = \sqrt{\frac{1}{n} \sum_{i=1}^n (\text{RSE}_i)^2} \quad (12)$$

where

$$\text{RSE} = \sqrt{\hat{\delta}_x^2 + \hat{\delta}_y^2} = \sqrt{(\hat{g}_x - G_x)^2 + (\hat{g}_y - G_y)^2} \quad (13)$$

denotes the root square error (RSE) of each VP, and (\hat{g}_x, \hat{g}_y) is the estimated coordinates of the reference VPs (RVPs) $G = (G_x, G_y)$. Low RMSE values correspond with a precise registration. Another metric of accuracy assessments to estimate errors in the entire image is the spatial mean error (SME) [35], [36], i.e.,

$$\text{SME} = \frac{1}{n} \sum_{h=1}^H n_h \text{SME}_h \quad (14)$$

where H is the number of strata, n is the number of VP pairs in the image, n_h is number of VPs in stratum h , and

$$\text{SME}_h = \frac{1}{n_h} \sum_{i=1}^{n_h} \text{RSE}_{h,i} \quad (15)$$

is the mean RSE of the VPs in stratum h .

According to the sampling of VPs in Fig. 3, the parameters in (14) are equal to $H = 16$, $n_h = 2$, and $n = 32$. In addition, the spatial variance (SV) of the estimated SME can be examined, without bias, as

$$\text{SV} = \sum_{h=1}^H \left(\frac{n_h}{n} \right)^2 \text{SV}_h + (\text{SME}^2) - (\text{SME})^2 \quad (16)$$

where SV_h is the estimated SV of SME_h , i.e.,

$$\text{SV}_h = \frac{1}{n_h(n_h - 1)} \sum_{i=1}^{n_h} (\text{RSE}_{h,i} - \text{SME}_h)^2 \quad (17)$$

$$\text{SME}^2 \frac{1}{n} \sum_{h=1}^H n_h \text{SME}_h^2 = \frac{1}{n} \sum_{h=1}^H \sum_{i=1}^{n_h} (\text{RSE}_{h,i})^2. \quad (18)$$

The SV is an important metric to assess the performance of the registration for remotely sensed images. Note that low SV values correspond with more uniform registration errors in the corrected image.

B. Results of Simulation Experiments

This section presents the simulation results to demonstrate the performance of the proposed method. By employing the setups in Section III-A, comparisons are made between the performances of the LS, WLS, TLS, STLS, and WTLS estimators, which are based on Monte Carlo simulations. Monte Carlo simulations explicitly represent uncertainties by specifying inputs as probability distributions [37]. To obtain a reliable estimation result, 10 000 Monte Carlo simulations for error addition and weight determination are carried out by generating random numbers from a specified probability distribution. Two problems are investigated in these simulations. First, we compare the performances of the unweighted estimators of the LS, TLS, and STLS methods, and the weighted estimators of the WLS and WTLS methods in estimating the model coefficients. Second, the simulation study demonstrates the difference in the registration errors of these estimators.

1) Coefficient Estimation Analysis: Table II presents the mean values and standard deviations of the coefficient estimations from the Monte Carlo simulations. Fig. 4 shows the variance, bias, and MSE of the estimated coefficient vectors $\hat{\beta}_x$ and $\hat{\beta}_y$ using different estimators. Table II and Fig. 4 illustrate the following.

The variances obtained with the WTLS estimation are equal to 0.1837 and 0.1905 m^2 in the x and y directions, respectively, whereas the variances of the other estimations are all above 0.6 m^2 . This indicates that the WTLS estimator is more robust in estimating model parameters. Apparently, the variances of the LS, TLS, and STLS estimators are fairly close to each other. In addition, we find that the variances in the x and y directions of the WLS coefficient estimation (0.6557 and 0.6380 m^2 , respectively) are slightly larger than those obtained by LS (0.6034 and 0.6290 m^2 , respectively), TLS (0.6038 and 0.6292 m^2 , respectively), and STLS (0.6036 and 0.6291 m^2 , respectively). This suggests that the one-sided weighted scheme of the WLS approach could not guarantee the robustness of parameter estimation when both the coordinates of the RCPs and the TCPs contain errors with different sizes.

The bias in the WTLS estimates is equal to 0.0008 and 0.0034 m in the x and y directions, respectively. These values are smaller than those from the other estimators. The reason is that the LS and WLS estimators are inconsistent and asymptotically biased if the RCP coordinates contain errors, whereas the TLS and STLS estimators assume that the errors obey a homoscedastic structure. Unfortunately, if there are points in the data set whose errors follow different probability distributions,

TABLE II
STATISTICAL RESULTS OF THE COEFFICIENT ESTIMATION FROM 10 000 MONTE CARLO SIMULATIONS

Coefficient	Direction	True values	Estimated values				
			LS	TLS	STLS	WLS	WTLS
$\hat{\beta}_0$	x	50	49.9975±0.7768	49.9700±0.7771	49.9865±0.7769	49.9982±0.8098	49.9992±0.4286
	y	50	49.9940±0.7931	49.9592±0.7932	49.9801±0.7932	49.9885±0.7988	49.9931±0.4365
$\hat{\beta}_1$	x	0.99	0.9900±0.0020	0.9901±0.0020	0.9900±0.0020	0.9900±0.0019	0.9900±0.0009
	y	0.1	0.1000±0.0020	0.1000±0.0020	0.1000±0.0020	0.1000±0.0019	0.1000±0.0009
$\hat{\beta}_2$	x	-0.1	-0.1000±0.0020	-0.1000±0.0020	-0.1000±0.0020	-0.1000±0.0019	-0.1000±0.0009
	y	0.99	0.9900±0.0020	0.9901±0.0020	0.9901±0.0020	0.9900±0.0019	0.9900±0.0009
$\hat{\beta}_3$	x	3e-5	(3.0000±0.1246)e-5	(2.9976±0.1246)e-5	(2.9991±0.1246)e-5	(2.9987±0.1301)e-5	(2.9998±0.0612)e-5
	y	3e-5	(2.9995±0.1253)e-5	(2.9960±0.1253)e-5	(2.9981±0.1253)e-5	(2.9993±0.1283)e-5	(2.9987±0.0615)e-5
$\hat{\beta}_4$	x	3e-5	(3.0000±0.1452)e-5	(2.9926±0.1452)e-5	(2.9971±0.1452)e-5	(2.9993±0.1371)e-5	(2.9994±0.0669)e-5
	y	-3e-5	(-3.0004±0.1449)e-5	(-3.0009±0.1449)e-5	(-3.0006±0.1449)e-5	(-3.0026±0.1366)e-5	(-3.0001±0.0664)e-5
$\hat{\beta}_5$	x	-3e-5	(-3.0006±0.1473)e-5	(-3.0000±0.1473)e-5	(-3.0004±0.1473)e-5	(-3.0006±0.1405)e-5	(-3.0005±0.0674)e-5
	y	3e-5	(2.9999±0.1469)e-5	(2.9923±0.1469)e-5	(2.9969±0.1469)e-5	(2.9998±0.1355)e-5	(2.9999±0.0670)e-5

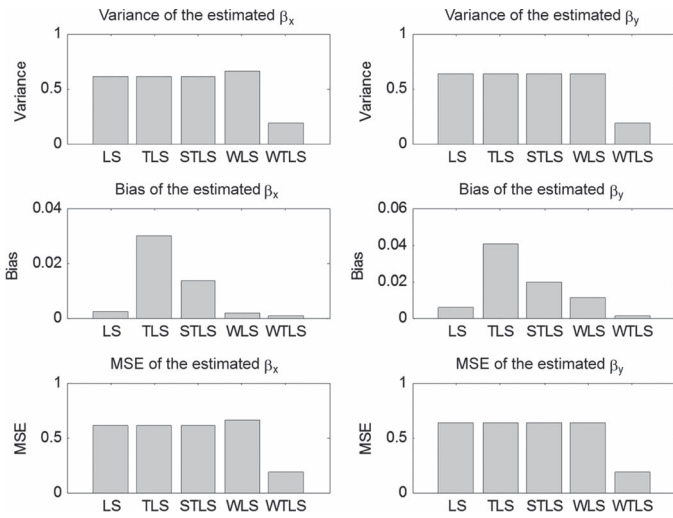


Fig. 4. Comparison of the estimated coefficients: Variance, bias, and MSE.

the homoscedastic error structure assumption of TLS and STLS cannot be satisfied, and they show poor performance. In contrast, the heteroscedastic error structure assumption and the two-sided weighted scheme of the WTLS estimator can guarantee low bias to a certain extent. Therefore, the WTLS estimator is more accurate in terms of parameter estimation.

Combining the effects of the variance and bias, we notice that the WTLS coefficient estimation has the lowest MSE. This is attributed to the robust coefficient estimates of the WTLS estimator that are not unduly affected by outliers or other small departures from the model assumptions. In summary, the WTLS estimator provides better coefficient estimations.

2) *Error Analysis:* To further investigate the performance of image registration, we next evaluate the accuracy metrics corresponding to registration errors, including the RMSE, the SME, and the SV of the SME.

Figs. 5, 6, and 7 present the RMSE, the SME, and the SV values collected from 10 000 Monte Carlo simulations at intervals of 200, respectively. Fig. 8 shows the mean RSE for each VP. The results of 10 000 Monte Carlo simulations are summarized in Table III. The following can be observed.

From the results in Figs. 5 and 8, and the quantitative statistical results in Table III, we observe that the RMSE and mean RSE of the WTLS method are smaller than those of the others. These differences illustrate large advantages of the WTLS estimator in reducing the registration error. Thus, in

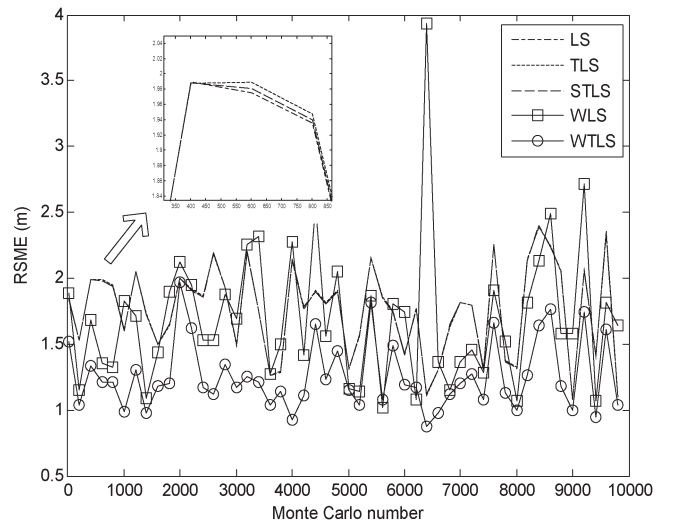


Fig. 5. RMSE in each Monte Carlo simulation.

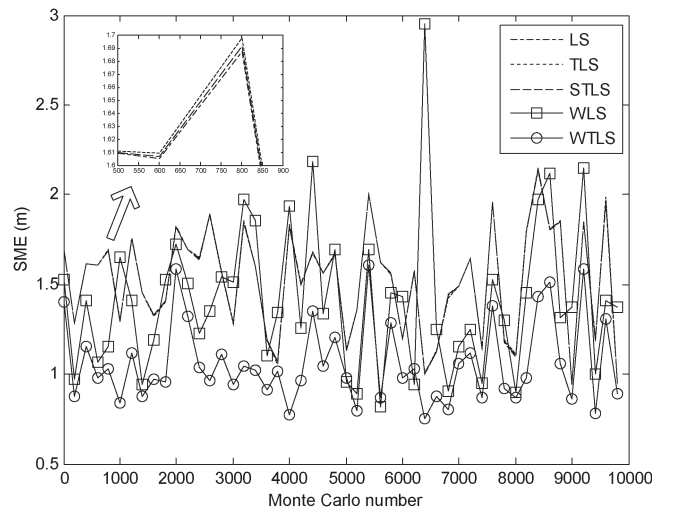


Fig. 6. SME in each Monte Carlo simulation.

terms of registration accuracy, WTLS clearly outperforms the unweighted LS, TLS, STLS, and one-sided weighted WLS methods. Meanwhile, the accuracy values of the LS, TLS, and STLS estimators are approximately equal to each other.

Fig. 6 and Table III show that the mean value of the SME obtained with WTLS equals 1.0693 m, whereas the mean values from using the other estimators are above 1.4 m. This suggests

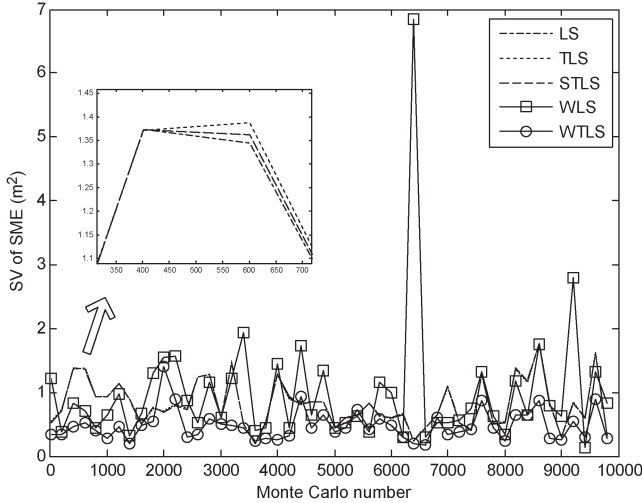


Fig. 7. SV of the SME in each Monte Carlo simulation.

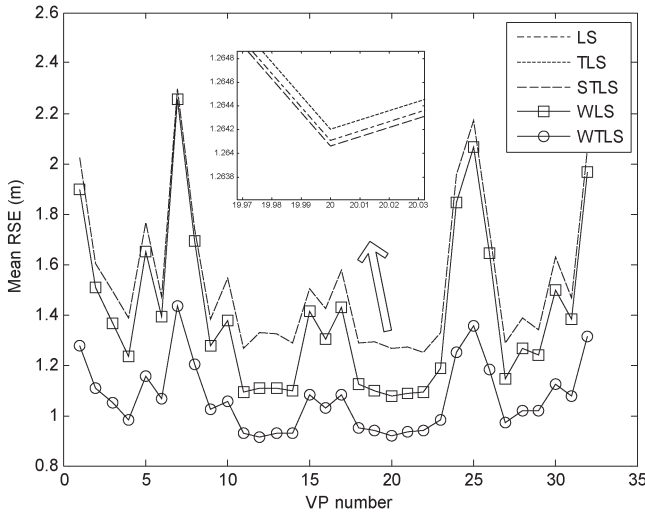


Fig. 8. Mean RSE of each VP from 10 000 Monte Carlo simulations.

TABLE III
STATISTICAL RESULTS OF THE RMSE, THE SME, AND THE SV FROM 10 000 MONTE CARLO SIMULATIONS

Estimator	RMSE (m)	SME (m)	SV (m ²)
LS	1.7626 ± 0.3261	1.5352 ± 0.2901	0.7878 ± 0.3742
TLS	1.7630 ± 0.3263	1.5356 ± 0.2903	0.7882 ± 0.3744
STLS	1.7626 ± 0.3262	1.5353 ± 0.2901	0.7879 ± 0.3742
WLS	1.6729 ± 0.5268	1.4040 ± 0.4282	0.9382 ± 0.8662
WTLS	1.2674 ± 0.2730	1.0693 ± 0.2395	0.4919 ± 0.2646

that the errors in the entire image via the WTLS method are lower.

Clearly, the SV of the WTLS estimator in Fig. 7 and Table III is smaller than those of the other estimators. It indicates that the WTLS estimator produces errors that are more stable and more evenly distributed than the error produced with the other estimators. The spatial distribution of the registered errors using the WTLS estimator is more uniform in the entire image.

The results in Figs. 5 and 6 illustrate that the WLS method does not always perform better than the LS method if the coordinates of the RCPs contain errors. Table III particularly shows that the SV of the WLS method (0.9382 m²) is the

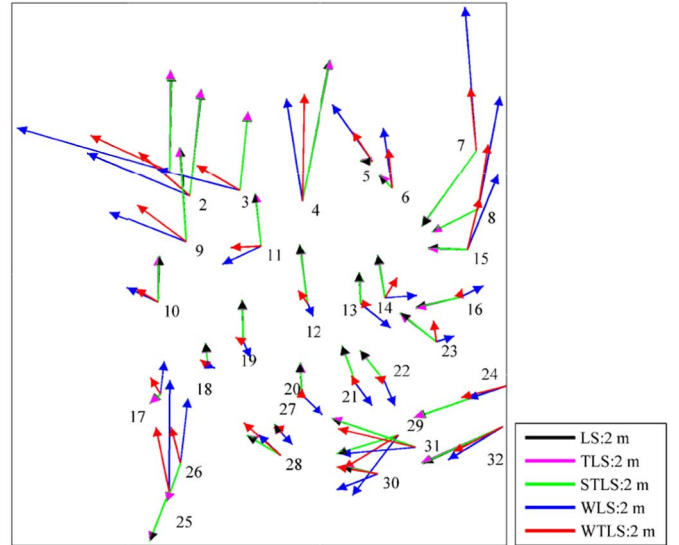


Fig. 9. Residual distribution map of one realization of the simulation experiments. The magnitude and direction of the RVPs' residuals are denoted by the arrow length and the direction, respectively.

largest among these methods, indicating that the registration errors of the WLS estimator are more widely spread apart and less uniformly distributed over the entire registered image. The one-sided weighted scheme, therefore, is not always effective in improving the registration when both the coordinates of the RCPs and the TCPs have noise of a different size. The results reveal that the WLS estimator cannot provide a globally uniform spatial pattern for image registration.

To further investigate the RCPs' residuals' distribution characteristics, we now discuss one particular realization among the Monte Carlo simulations. After the registration, the residuals for each RVP are shown in Fig. 9. The black, pink, green, blue, and red arrows represent the residuals obtained from the LS, TLS, STLS, WLS, and WTLS estimators, respectively, with the arrow length and the direction representing the magnitude and direction of the RVP residuals, respectively.

To evaluate the differences in these residuals, for the mean and variance of the residuals from estimators E_1 and E_2 , we have the following hypotheses:

$$H_{10} : \text{mean}_{E_1} \geq \text{mean}_{E_2} \text{ vs } H_{11} : \text{mean}_{E_1} < \text{mean}_{E_2} \quad (19)$$

$$H_{20} : \text{variance}_{E_1} \geq \text{variance}_{E_2} \text{ vs } H_{21} : \text{variance}_{E_1} < \text{variance}_{E_2}. \quad (20)$$

Z-statistics and F-statistics are then computed for the aforementioned two types of hypotheses as follows:

$$Z = \frac{\bar{\gamma}_{E_1} - \bar{\gamma}_{E_2}}{\sqrt{S_{E_1}^2/n_{E_1} + S_{E_2}^2/n_{E_2}}} \quad (21)$$

$$F = S_{E_1}^2/S_{E_2}^2 \quad (22)$$

where $\bar{\gamma}$ and S are the mean and standard deviation of the CPs' residuals, respectively, and n is the number of CP pairs. Hence, H_{10} holds if and only if $Z \geq -Z_{\alpha/2}(\min(n_{E_1} - 1, n_{E_2} - 1))$, whereas H_{20} holds if and only if $F \leq F_{\alpha/2}(n_{E_1} - 1, n_{E_2} - 1)$, where $Z_{\alpha/2}(\min(n_{E_1} - 1, n_{E_2} - 1))$ and $F_{\alpha/2}(n_{E_1} - 1, n_{E_2} - 1)$ are given critical values. Since $\alpha = 0.05$ and

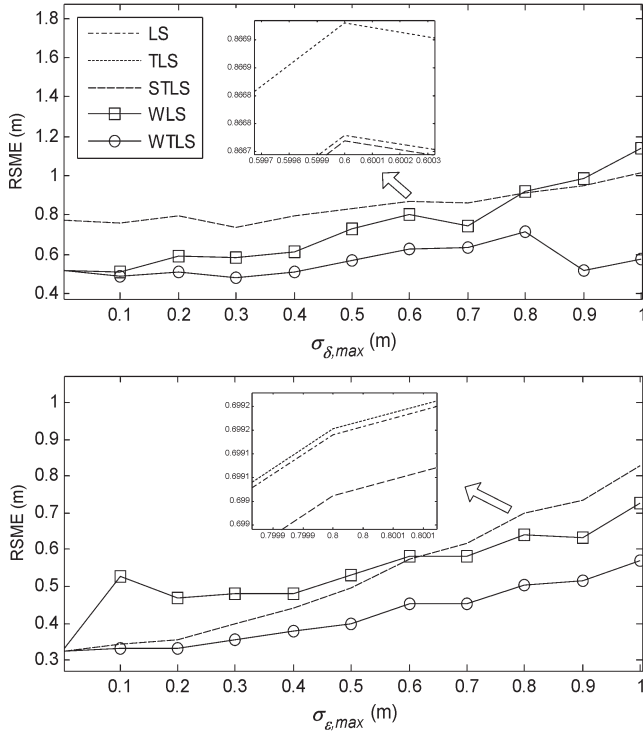


Fig. 10. RMSE of image registration with the increasing of maximal standard deviations $\sigma_{\delta, \max}$ and $\sigma_{\varepsilon, \max}$ in the simulated image experiment.

$n_{E_1} = n_{E_2} = 64$, the critical values are $Z_{0.025}(63) = 1.671$ and $F_{0.025}(63, 63) = 1.534$, respectively. Under these conditions, the hypotheses that the mean and variance of the residuals from WTLS are smaller than those from the others are accepted by comparing the quantitative Z -statistics and F -statistics with the critical values. These support the assertion that the residuals of WTLS are smaller and distributed more unevenly than those obtained with other estimators.

3) *Sensitivity Analysis*: To assess the robustness of the registration using the method proposed in this paper, a sensitivity analysis is further carried out by changing the predetermined values of the maximal standard deviations $\sigma_{\delta, \max}$ and $\sigma_{\varepsilon, \max}$ in simulations. With a different pair of $\sigma_{\delta, \max}$ and $\sigma_{\varepsilon, \max}$, the distribution of generating the random error added in CPs is accordingly different from each other and, then, makes the accuracy of the registration vary in size. By the aforementioned simulations, the effects of the uncertainties in the CPs' measured coordinates on the stability of the registration with different estimators can be investigated.

The plots of the mean RMSE during 10 000 Monte Carlo simulations versus $\sigma_{\delta, \max}$ and $\sigma_{\varepsilon, \max}$ are then analyzed in Fig. 10. Table IV presents the averages of the relative change rates of the RMSE with the intervals $\Delta\sigma_{\delta, \max} = \Delta\sigma_{\varepsilon, \max} = 0.1$. The result shows that the WTLS estimator provides a lower and more stable RMSE than those from other methods as the maximal standard deviations increase. In addition, it can be found that the WTLS-based registration method is insensitive to the choice of the distribution of random errors in CPs.

In summary, the WTLS estimator is more accurate and robust than the other estimators for simulated image registration. The LS and WLS estimators cannot effectively deal with the errors existing in RCPs, whereas TLS and STLS obtain similar

TABLE IV
AVERAGES OF THE RELATIVE CHANGE RATES OF THE RMSE
WITH THE INTERVALS $\Delta\sigma_{\delta, \max} = \Delta\sigma_{\varepsilon, \max} = 0.1$

Estimator	$d_{\delta}^{RMSE_a}$	$d_{\varepsilon}^{RMSE_b}$
LS	0.4689	0.8891
TLS	0.4697	0.8889
STLS	0.4688	0.8891
WLS	0.9245	0.9562
WTLS	0.4181	0.4558

$$a \quad d_{\delta}^{RMSE} = \frac{1}{n} \sum_{i=1}^n \frac{RMSE_{i+1} - RMSE_i}{RMSE_{i+1}} / \Delta\sigma_{\delta, \max}, \quad n \text{ is the number of intervals,}$$

$RMSE_i$ is the mean values of RMSE in 10000 Monte Carlo simulations with the i th $\sigma_{\delta, \max}$;

$$b \quad d_{\varepsilon}^{RMSE} = \frac{1}{n} \sum_{i=1}^n \frac{RMSE_{i+1} - RMSE_i}{RMSE_{i+1}} / \Delta\sigma_{\varepsilon, \max}, \quad n \text{ is the number of intervals,}$$

$RMSE_i$ is the mean values of RMSE in 10000 Monte Carlo simulations with the i th $\sigma_{\varepsilon, \max}$

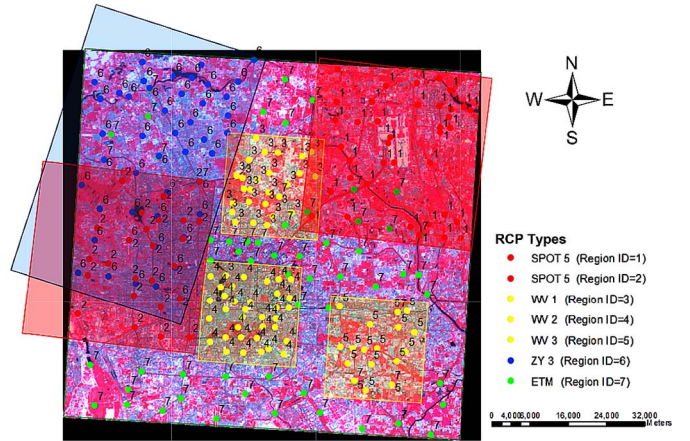


Fig. 11. Real remotely sensed image (data set A) for the registration and distribution of 248 points from different types of remote sensors.

results with LS when heteroscedastic errors exist in the measured CPs.

IV. EXPERIMENTS WITH REMOTELY SENSED IMAGES

Compared with simulated images, the geometric distortion of remotely sensed images is more complex. For example, feature points in images are often difficult to identify and match, particularly in images with different spatial resolutions. The geometric distortion may result in RCPs with different accuracy values that consequently influence the accuracy obtained during image registration. Furthermore, in practical applications, the acquisition of an entire reference image for registration may be difficult and costly. It might be more convenient to collect pairs of CPs from multiple reference images than from a single reference image. This may then lead to measurement errors in the coordinates of CPs that are of different sizes; thus, the accuracy of CPs is different from each other. This section describes the performance of the WTLS-based registration approach for remotely sensed images.

TABLE V
DESCRIPTION OF MULTIPLE REFERENCE IMAGES IN DATA SET A

Image type	Symbol color	Region ID	Spatial resolution	Acquisition time	Size (pixels)
SPOT 5 ^a	Red	1	2.5 m	Nov. 7, 2002	6876×7390
SPOT 5	Red	2	2.5 m	Nov. 7, 2002	6876×7543
WV 2 ^b	Yellow	3	2.0 m	Nov. 20, 2011	5173×5184
WV 2	Yellow	4	2.0 m	Nov. 20, 2011	5156×5148
WV 2	Yellow	5	0.5 m	Nov. 20, 2011	20576×21017
ZY 3 ^c	Blue	6	5.8 m	Apr. 17, 2012	6000×7200
ETM ^d	Green	7	15.0 m	Oct. 6, 2011	4000×4000

^a Système Probatoire d'Observation de la Terre 5

^b World View 2

^c Satellite Surveying and Mapping Application Center (SBSM) Zi Yuan 3 satellite

^d Enhanced Thematic Mapper in Landsat 7 satellite

A. Experiments Using Remotely Sensed Images

1) Image Description:

a) Data set A: We first analyze images from the Beijing-1 (BJ-1) small satellite. The BJ-1 small satellite, as one component of the Disaster Monitoring Constellation, was put into use in 2005 and has been widely used in China. It carries two payloads that provide high-resolution (4 m) panchromatic images alongside medium-resolution (32 m) three-band multispectral images with an ultrawide 600-km imaging swath [38]. Its panchromatic imager is of the push-broom type. In order to ensure true utility for its satellite data, geometric precise rectification is a key component to deal with. Fig. 11 shows a BJ-1 small satellite multispectral image acquired over Beijing, China, on July 11, 2011. The size is 1460×1366 pixels. The upper-left longitude and latitude coordinates of this image are $116^{\circ}1'51.03''$ E and $40^{\circ}0'39.87''$ N, respectively; and the lower-right longitude and latitude coordinates are $116^{\circ}1'30.83''$ E and $39^{\circ}6'11.63''$ N, respectively. Less than 1/20 of this study area is covered with mountains, and the elevation range of this area is from 38 to 189 m. It indicates that this region is generally flat; thus, it can be supposed that no distortion problems are caused by terrain effects.

To match the area of the distorted image (see Fig. 11), seven regions of reference images are obtained from multiple sources, including four types of remotely sensed images, as described in Table V. These reference images have different spatial resolutions and overlap areas on the distorted image. The cover areas of these images over the distorted image are also shown in Fig. 11.

b) Data set B: The second data set contains remote sensing images from Tianjin Port along the coast of the Bohai Sea. This data set is used to investigate the performance of the WTLS estimator. Tianjin Port is a major transport hub in the thriving Chinese economy. With the rapid increase in import and export throughput, land use at this trade port has dramatically changed over the last five years. Since the change of land use can influence sectors such as housing, infrastructure, and development space, it is crucial to quickly monitor its changes. Change detection techniques with remotely sensed images are often used to monitor land-use changes over a period of time. There is, however, a recurrent distortion between remote sensing images from different phases that may affect the drawing of correct conclusions. Hence, before carrying out a change detection analysis, geometric registration must be implemented.

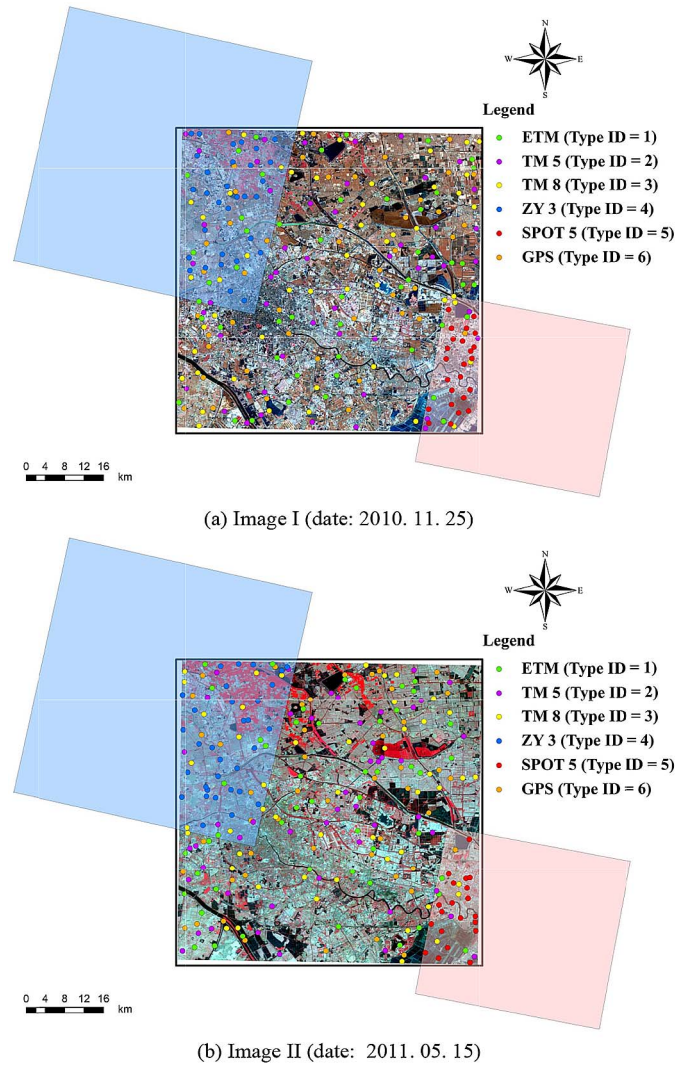


Fig. 12. Real remotely sensed images (data set B) for the registration and distribution of points from different types of remote sensors. (a) Image I (date: November 25, 2010). (b) Image II (date: May 15, 2011).

TABLE VI
DESCRIPTION OF MULTIPLE REFERENCE IMAGES IN DATA SET B

Data type	Symbol color	Type ID	Spatial resolution	Acquisition time	Size (pixels)
ETM ^a	Green	1	15 m	May. 18, 2003	4135×4136
TM 5 ^b	Purple	2	30 m	Apr. 27, 2010	2068×2068
TM 8 ^c	Yellow	3	30 m	Feb. 5, 2013	2068×2068
ZY 3 ^d	Blue	4	5.8 m	Aug. 23, 2012	14018×11265
SPOT 5 ^e	Red	5	2.5 m	Jun. 2, 2009	12002×14002
GPS ^f	Orange	6	1 m	Dec. 14, 2013	--

^a Enhanced Thematic Mapper in Landsat 7 satellite

^b Thematic Mapper in Landsat 5 satellite

^c Thematic Mapper in Landsat 8 satellite

^d Global Positioning System (version: UNISTRONG JiSiBao MG838)

In particular, an absolute registration of multiple images by geometric correction in the same geographic coordinate system is important for monitoring a change trend over a long period.

In this experiment, two BJ-1 multispectral images with three channels acquired over a same area in Tianjin Port on November 25, 2010 and May 15, 2011 are taken as uncorrected remotely sensed data (see Fig. 12). The sizes of the images are 1975×2017 and 1941×1950 pixels, respectively. For the absolute registration, five precise geocorrected images and

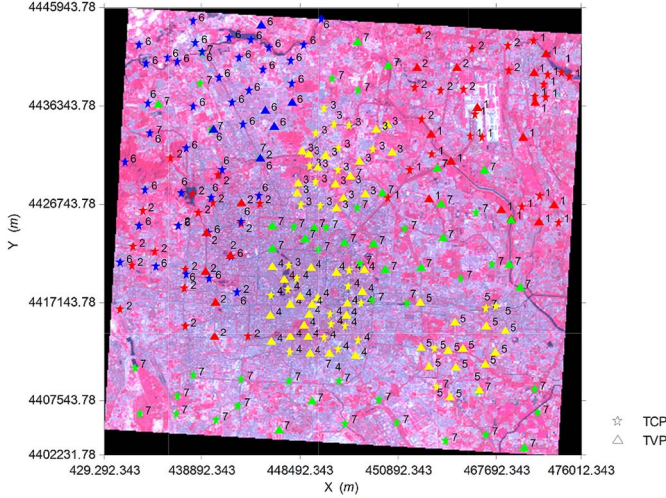


Fig. 13. Distribution of the selected TCPs and TVPs in the real remotely sensed image experiment (data set A). The numbers near the labels represent their region ID.

a series of observed points obtained by GPS precise point positioning are taken as reference data (see Table VI). The reference data of the ETM, TM 5, and TM 8 images can cover the whole distorted image. The GPS observed points in this experiment can be uniformly distributed over the uncorrected data. The cover area of the *Système Probatoire d’Observation de la Terre 5* (SPOT 5) image is located in the lower-right corner of the distorted image, whereas the *Zi Yuan 3* (ZY 3) image is located in the opposite direction (see Fig. 12). Note that the study area of this data set lies on the coast of the Bohai Sea. Hence, no terrain distortion is considered as the land flattens out near the coast.

2) *Image Registration With IRTLS*: Similar to the simulation study, the registration of remotely sensed images mainly comprises the following four steps.

a) *Model selection*: An appropriate model should be selected first. Considering the relative flatness in the study area and the deformation characteristics in Figs. 11 and 12, we adopt a second-order EIV model to correct the geometric deformation of the distorted images.

b) *CPs’ collection and weight determination*: Point pairs are collected in the multiple reference images and the distorted image. In Figs. 11 and 12, the point pairs with their types of satellites are also shown. The accuracy of each of these points is unequal to each other, and their relative importance for registration is accordingly different and weighted. In the simulation experiments, the differences in the accuracy of the RCPs and that of the TCPs are known. In this remotely sensed image experiment, however, they cannot be available or accurate even if available. Thus, the appropriate variance values σ_ε^2 and σ_δ^2 , and the exact weights are unknown. The estimated weights for WTLS should be then used. Consequently, a method for adaptively optimizing and determining weights in the WTLS estimator is developed to guarantee its practicability.

Iteratively reweighted LS (IRLS) is used to determine the weights for the WLS estimator [39]–[41]. It adaptively estimates the weights of a response variable and thus obtains an accurate regression result. We generalize this concept to the WTLS estimator for determining both the weights of response variables and those of the explanatory variables.

In the initialization step, identical weights are set to each pair of CPs to perform WTLS. In the update step, similar to the optimization in IRLS, a reweighting scheme for both the explanatory and response variables is designed to estimate the weights. Its core idea is that squared residual regression is resorted to estimate the weights for the next step after extracting the residuals of the coordinates of the RCPs and the TCPs. First, the squared residuals $\tilde{\varepsilon}^2$ and $\tilde{\delta}^2$ in the TCPs and the RCPs are computed. The actual unknown squared errors ε^2 and δ^2 are then estimated by regressing $\tilde{\varepsilon}^2$ and $\tilde{\delta}^2$ using LS. After that, the estimated values of squared errors $\hat{\varepsilon}^2$ and $\hat{\delta}^2$ are used to fit variances $\hat{\sigma}_\varepsilon^2 = 1/\hat{\varepsilon}^2$ and $\hat{\sigma}_\delta^2 = 1/\hat{\delta}^2$. These fitted values are further used to replace the unknown variances σ_ε^2 and σ_δ^2 . Then, the estimated weights are updated with

$$\begin{cases} \hat{w}_\varepsilon = \sigma_0^2 / \hat{\sigma}_\varepsilon^2 \\ \hat{w}_\delta = \sigma_0^2 / \hat{\sigma}_\delta^2 \end{cases} \quad (23)$$

and used in the next iteration step. This is repeated until convergence is reached, which usually happens after only a few iterations. Note that the weights for the RCPs and the TCPs are adaptively recomputed by this iterative scheme in which each step involves solving a WTLS problem. As an approach to deal with the heteroscedasticity in the EIV model, we call this algorithm the IRTLS. A detailed description of the iteratively reweighted scheme can be found in [40] and [41].

c) *Model estimation and image registration*: The LS, IRLS, and IRTLS approaches are used to estimate the parameters of a second-order EIV model. To do so, 20 iterations are run in the loop of the IRTLS algorithm. Based on the estimations by this approach, resampling technologies are employed to perform image registration.

d) *Accuracy assessment*: The statistical evaluation of the registration is generalized based on VPs. For the accuracy assessment metrics in the simulation experiment, the prerequisite is the availability of the true values of coefficients $\beta = (\beta_x, \beta_y)$ or the true coordinates $G = (G_x, G_y)$ of the RVPs. For remotely sensed images, however, such prior information is unknown. The observed coordinates $g = (g_x, g_y)$ of the RCPs are commonly used to replace true coordinates $G = (G_x, G_y)$ to obtain the RMSE. That is, the RSE of each VP in (12) is calculated as

$$\begin{aligned} \text{RSE} &= \sqrt{\tilde{\delta}_x^2 + \tilde{\delta}_y^2} \\ &= \sqrt{(\hat{g}_x - \tilde{G}_x)^2 + (\hat{g}_y - \tilde{G}_y)^2} \\ &= \sqrt{(\hat{g}_x - g_x)^2 + (\hat{g}_y - g_y)^2}. \end{aligned} \quad (24)$$

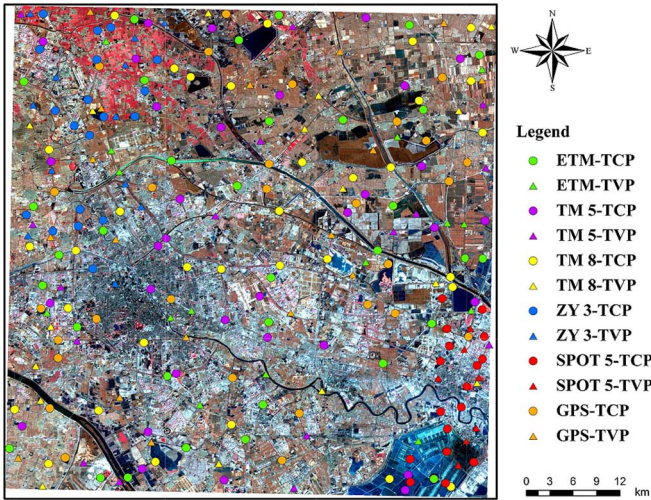
Nevertheless, the objective of the LS estimator is to minimize the sum of the squares of residual errors, which is consistent with the minimization of the RMSE using (24). Therefore, if the differences between the observed coordinates $g = (g_x, g_y)$ and the true coordinates $G = (G_x, G_y)$, i.e.,

$$\begin{aligned} \text{Difference}(g, G) &= \sqrt{\delta_x^2 + \delta_y^2} \\ &= \sqrt{(g_x - G_x)^2 + (g_y - G_y)^2} \end{aligned} \quad (25)$$

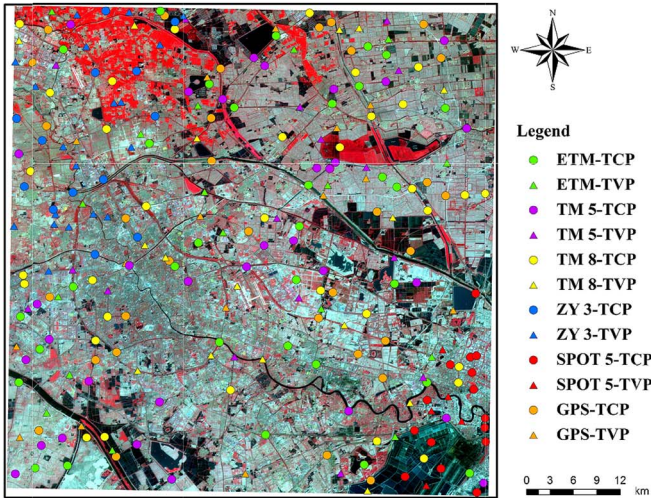
are insufficiently small, the approximation in (24) for computing the RMSE cannot be justified to compare the accuracy of LS with that of the other methods.

TABLE VII
RESULTS OF THE COEFFICIENT ESTIMATION, THE RMSE, AND THE SV FROM THE EXPERIMENT WITH DATA SET A

Estimator	Direction	$\hat{\beta}_0$	$\hat{\beta}_1$	$\hat{\beta}_2$	$\hat{\beta}_3$	$\hat{\beta}_4$	$\hat{\beta}_5$	RMSE (m)	SV (m ²)
LS	x	43.3276	0.0313	-0.0019	4.5618e-10	-2.6700e-9	1.7202e-9	23.8753	141.9094
	y	-41.8243	0.0018	0.0315	-3.1508e-9	1.0781e-9	-4.1468e-9		
IRLS	x	43.3036	0.0313	-0.0019	2.7006e-10	-2.2284e-9	8.9441e-10	22.8319	112.8319
	y	-41.4198	0.0018	0.0314	-2.6686e-9	9.3246e-10	-3.2379e-9		
IRTLS	x	43.4630	0.0312	-0.0018	5.3082e-10	-7.6142e-10	-2.2841e-10	17.5869	40.6272
	y	-39.6559	0.0018	0.0312	-4.01889e-10	2.7219e-11	-3.3567e-12		



(a) Image I (date: 2010. 11. 25)



(b) Image II (date: 2011. 05. 15)

Fig. 14. Distribution of the selected TCPs and TVPs in the real remotely sensed image experiment (data set B). (a) Image I (date: November 25, 2010). (b) Image II (date: May 15, 2011).

To overcome this problem, we selected 98 pairs of VPs from the 248 pairs of points for data set A. The residuals of these VPs are requested to be less than one pixel. The remaining 150 pairs of points are employed as CPs for estimations. That is, among the 248 pairs of points, the more accurate points are employed as VPs, the less accurate points are used to calculate the parameters of models. The distributions of the RCPs and the RVPs are shown in Fig. 13. Following similar principles and procedures, we selected 163 pairs of CPs and 83 pairs of VPs for the experiment with Image I in data set B. We collected

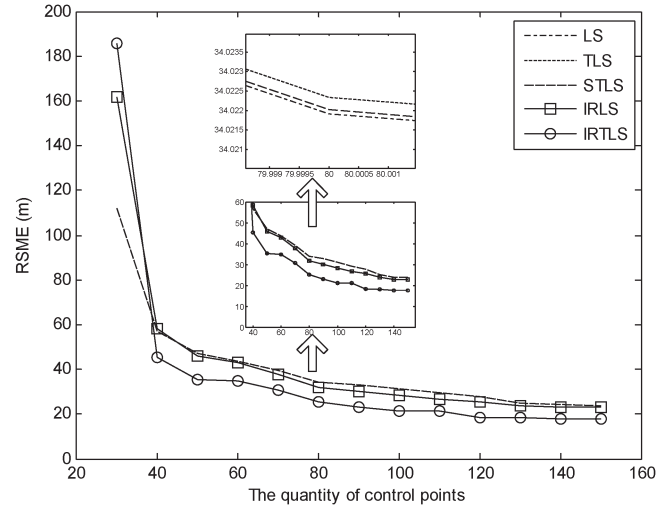


Fig. 15. RMSE of image registration for the LS, IRLS, and IRTLS estimators with the increase in CPs' number in the real remotely sensed image experiment.

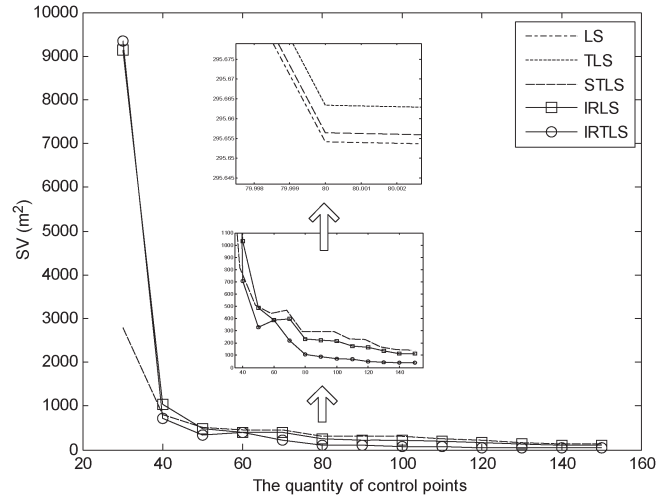


Fig. 16. SV of image registration for the LS, IRLS, and IRTLS estimators with the increase in CPs' number in the real remotely sensed image experiment.

158 pairs of CPs and 88 pairs of VPs for Image II. Fig. 14 presents the distributions of different sources' TCPs and TVPs on the distorted images.

B. Results of Remotely Sensed Image Experiment

1) Data Set A: The estimates from the IRTLS method theoretically converge to true values as the number of samples n tends to infinity. Hence, this paper first demonstrates the effect of the number of CPs and compares the performance of the LS, TLS, STLS, IRLS, and IRTLS approaches with different numbers of CPs.

TABLE VIII
RESULTS OF THE COEFFICIENT ESTIMATION, THE RMSE, AND THE SV FROM THE EXPERIMENT WITH DATA SET B

Image	Estimator	Direction	$\hat{\beta}_0$	$\hat{\beta}_1$	$\hat{\beta}_2$	$\hat{\beta}_3$	$\hat{\beta}_4$	$\hat{\beta}_5$	RMSE (m)	SV (m ²)
Image I (date: 2010.11.25)	LS	x	14.5477	0.9731	-0.0273	9.4476e-10	-2.2356e-9	6.2152e-10	12.1324	74.2349
		y	19.6721	0.1476	0.6326	-6.4245e-10	8.4374e-9	-9.4389e-10		
	IRLS	x	15.6857	0.9321	-0.0322	8.7311e-10	-7.6541e-10	5.6413e-10	11.0155	67.8132
		y	19.1454	0.1393	0.8333	-1.5575e-9	4.6541e-9	-4.6583e-10		
	IRTLS	x	14.7819	0.8769	-0.0477	9.4894e-11	-8.3752e-12	-5.7688e-10	9.3790	48.9916
		y	20.2356	0.1140	0.9648	-2.8705e-10	8.6344e-9	-3.7047e-11		
Image II (date: 2011.05.15)	LS	x	15.1621	0.8784	-0.0385	5.4527e-9	-6.3705e-10	7.6541e-10	10.4365	62.0322
		y	20.8830	0.0387	0.8776	-8.8536e-10	2.3638e-10	-4.1147e-10		
	IRLS	x	14.4150	0.8785	-0.0396	4.4111e-9	-2.9093e-10	6.6743e-10	9.3158	46.0373
		y	20.4125	0.0388	0.8775	-9.5575e-10	9.5271e-10	-3.1234e-10		
	IRTLS	x	14.5261	0.8696	-0.0496	5.4192e-10	-7.6526e-10	-2.5324e-10	7.4778	17.2743
		y	20.3236	0.0497	0.8887	-4.5436e-10	6.5786e-11	-3.4568e-12		



Fig. 17. Corrected image using the IRTLS approach for the experiment with data set A.

Figs. 15 and 16 compare the RMSE and SV of these different approaches with different numbers of CPs. These figures show that an increase in the number of CPs has a positive effect on the registration accuracy to a varying degree. For IRTLS, the changes in the RMSE and the SV from 10 to 80 CPs are equal to 160.2131 m and 288.3127 m², respectively, whereas the improvement in the RMSE and the SV from 80 to 150 CPs only equals 7.6 m and 2.1032 m², respectively. Furthermore, the IRTLS method is more effective under a large-sample theory. As shown in Figs. 15 and 16, the results of IRTLS are poor when the quantity of CPs is below 40. The RMSE and SV of the IRTLS estimator, however, fall at a fast rate as the number of CPs increases. Higher accuracy of IRTLS will be more pronounced as the quantity of CPs increases. When the quantity of CPs is larger than 40, IRTLS performs better than the other estimators in terms of the RMSE and the SV. More samples would be needed to guarantee its consistency. We conclude that the number of CPs affects registration accuracy and that it is important to only use IRTLS with a sufficiently large number of CPs. Clear dominance of this estimator over others is apparent for a large number of CPs. Other estimators cannot estimate the

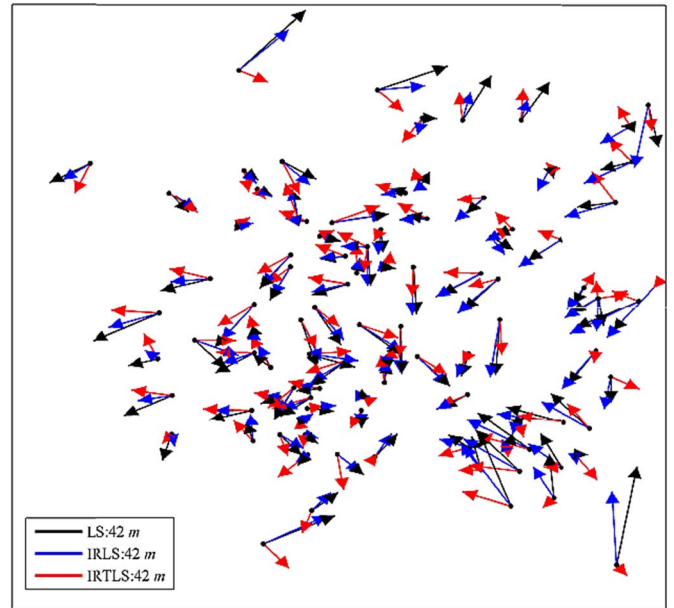


Fig. 18. Residual distribution map for the experiment with data set A. The magnitude and direction of the RVPs' residuals are denoted by the arrow length and the direction, respectively.

model parameters at high precision since they heavily rely on assumptions that cannot be met in this application.

Subsequently, the results of using 150 CPs are presented to further evaluate the methods. Table VII shows the results for the registration. In a noisy environment, there are decreases of 26.34% and 22.97% in the RMSE values and decreases of 77.37% and 63.99% in the SV values when comparing IRTLS with LS and IRLS, respectively. It is concluded from Table VII that the errors in the RCPs would partly result in the inaccurate estimation of coefficients in LS and IRLS that only consider random errors in the coordinates of the TCPs without RCPs. The accuracy in the coefficient estimation of IRTLS is more pronounced. Fig. 17 presents the final corrected image using IRTLS with nearest neighbor resampling. The coordinate systems is World Geodetic Survey 1984, and the map projection is the Universal Transverse Mercator projection.

Fig. 18 shows the distribution of the residuals of the RVPs. Based on Fig. 18, hypothesis tests between the IRTLS estimator and the other estimators support the claim that the residuals

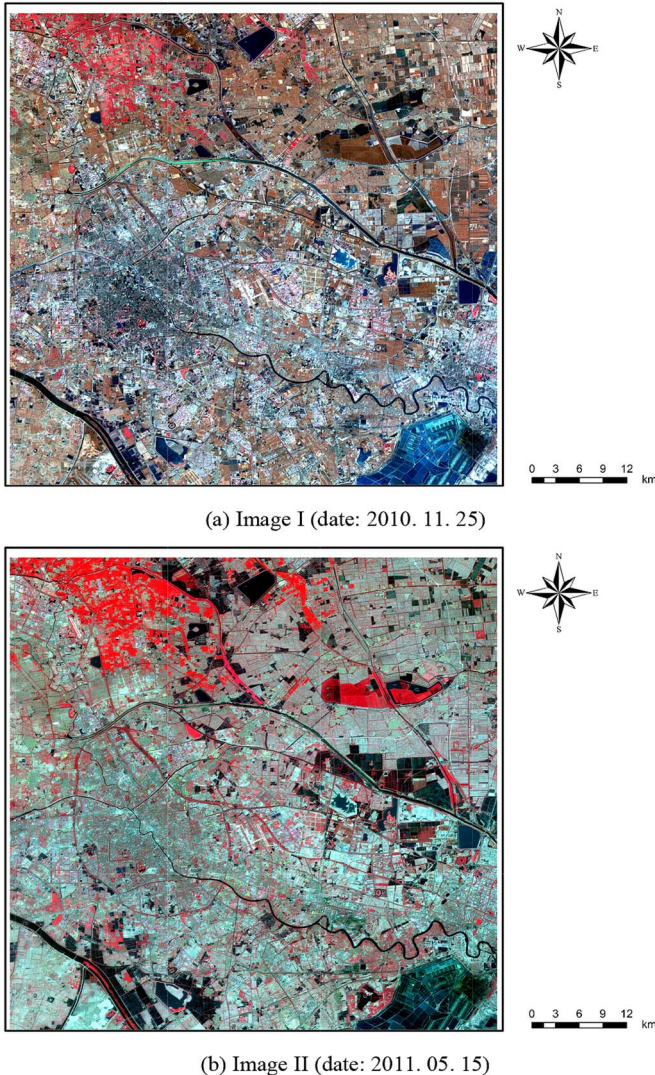


Fig. 19. Corrected images using the IRTLS approach for the experiment with data set B. (a) Image I (date: November 25, 2010). (b) Image II (date: May 15, 2011).

from IRTLS are smaller and are more evenly distributed than the other two methods. That is, the residual errors throughout the entire registered images are more homogeneous with the IRTLS method. The effect of the residuals on subsequent operations such as multisource data fusion and change detection can be reduced.

2) *Data Set B*: The registration process of data set B is similar to that of data set A. Comparative results are also presented with this data set. Table VIII shows the results of the registrations and specifies that there are decreases of 14.8534% (Image I) and 19.7299% (Image II) in the RMSE by comparing IRTLS with IRLS and decreases of 22.6946% (Image I) and 28.3495% (Image II) in the RMSE by comparing IRTLS with LS. Meanwhile, IRTLS obtains lower SV values on this data set, which suggests that the registration errors contained in the corrected image (see Fig. 19) using the IRTLS estimator are more likely to follow a uniform distribution, i.e., residuals are more homogeneous when applying IRTLS throughout the entire registration period of the images. Consequently, less error will propagate to the results of change detection between the

two images, and a more accurate land-use change of the area is monitored over the study period.

C. Discussions

In this experiment, the proposed IRTLS method was validated as a reliable registration method for remotely sensed images. The cause is that the error structure in the IRTLS method relaxes into a heteroscedastic pattern. Based on this, two-sided weights can be used to describe the varying importance of RCPs and TCPs that are of different accuracy.

We note that the spatial resolution of an uncorrected image equals 32 m, whereas the spatial resolution of the reference images varies from 0.5 to 15 m. When manually collecting CPs, the locations of RCPs corresponding to TCPs are difficult to accurately determine owing to the different resolutions between the distorted images and the reference images. Therefore, positioning errors are still introduced even under the assumption that all correspondences are correct (i.e., no mismatch is considered), which will influence the registration results to a certain degree. Then, the errors in the residuals of the RCPs might propagate from the positioning errors to the entire registered images. If the scales of the spatial resolution are similar, it is relatively convenient to accurately locate pairs of CPs from distorted images and reference images. If the difference of spatial resolutions is large, however, it is relatively difficult to accurately fix the positions of RCPs from reference images. Such positioning errors would reduce the accuracy of model estimation. The two-sided weighted scheme in our IRTLS method partly reduces the effect of CPs' positioning errors. Positioning errors from multiscale reference images are worthy to be further investigated, particularly their influences on the registration results and the analysis on how robust our approach is to mismatches. In addition, at this stage, it is unknown whether the techniques can be expanded to other types of images, such as high-resolution images, oblique images, or SAR images. We plan to do further research on these data sets in the future.

It was assumed that all CPs are independently collected in the experiments. Because of spatial autocorrelation in the remotely sensed imagery, however, covariance and weight matrices differ from diagonal matrices. Therefore, a general IRTLS method to handle CPs with spatial autocorrelation needs to be developed in the near future.

V. CONCLUSION

This paper has introduced the EIV-model-based IRTLS estimator into image registration for RCPs and TCPs of which the coordinates contain heteroscedastic errors. By comparing the variance, bias, and MSE of the coefficient estimations obtained from Monte Carlo simulations, this paper has demonstrated that the coefficient estimates obtained by the WTLS-based estimator were more accurate and robust than those obtained by the LS, WLS, TLS, and STLS estimators if both the coordinates of RCPs and TCPs contain errors of different sizes. The registration errors from the WTLS-based estimation were lower in magnitude and more uniform in distribution, as expressed by the RMSE, the SME, and the SV. By employing a novel adaptive weight determination scheme, a reliable registration for remotely sensed images was achieved. The quantity of CPs was

validated as a critical factor that affects the use of the estimator in registration applications. The results showed that, for a large number of CPs, the proposed IRTLS method has a superior performance over the general methods in terms of registration accuracy and residual uniformity. With these attributes, the IRTLS method is considered an effective and reliable technique for image registration when the coordinates of RCPs and TCPs contain heteroscedastic errors. Therefore, it is recommended that our presented approach is further expanded and used in the registration of remotely sensed imagery in order to obtain higher accuracy and greater reliability.

ACKNOWLEDGMENT

The authors would like to thank the four anonymous reviewers for their constructive comments that have helped improve this paper.

REFERENCES

- [1] T. Toutin, "Review article: Geometric processing of remote sensing images: Models, algorithms and methods," *Int. J. Remote Sens.*, vol. 25, no. 10, pp. 1893–1924, 2004.
- [2] B. Zitov and J. Flusser, "Image registration methods: A survey," *Image Vis. Comput.*, vol. 21, no. 11, pp. 977–1000, Oct. 2003.
- [3] R. S. Lunetta, R. G. Congalton, L. R. Fenstermaker, K. C. McGwire, and L. R. Tinney, "Remote sensing and geographic information system data integration: Error sources and research issues," *Photogramm. Eng. Remote Sens.*, vol. 57, no. 6, pp. 677–687, Jun. 1991.
- [4] Y. Ge, Y. Leung, J. H. Ma, and J. F. Wang, "Modeling for registration of remotely sensed imagery when reference control points contain error," *Sci. China Series D-Earth Sci.*, vol. 49, no. 7, pp. 739–746, 2006.
- [5] S. Van Huffel and J. Vandewalle, *The Total Least Squares Problem: Computational Aspects and Analysis*. Philadelphia, PA, USA: SIAM, 1991.
- [6] S. Van Huffel, Ed., *Recent Advances in Total Least Squares Techniques and Errors-in-Variables Modeling*. Philadelphia, PA, USA: SIAM, 1997.
- [7] S. Van Huffel and P. Lemmerling, Eds., *Total Least Squares and Errors-in-Variables Modeling: Analysis, Algorithms and Applications*. Dordrecht, The Netherlands: Kluwer, 2002.
- [8] I. Markovsky and S. Van Huffel, "Overview of total least squares methods," *J. Signal Process.*, vol. 87, no. 10, pp. 2283–2302, Oct. 2007.
- [9] B. Matei and P. Meer, "Estimation of nonlinear errors-in-variables models for computer vision applications," *IEEE Trans. Pattern Anal. Mach. Intell.*, vol. 28, no. 10, pp. 1537–1552, Oct. 2006.
- [10] C. C. Paige and Z. Strakoš, "Scaled total least squares fundamentals," *Numer. Math.*, vol. 91, no. 1, pp. 117–146, Mar. 2002.
- [11] Y. Ge, T. J. Wu, J. H. Wang, J. H. Ma, and Y. Y. Du, "Scaled total-least-squares-based registration for optical remote sensing imagery," *Earth Sci. Informat.*, vol. 5, no. 3/4, pp. 137–152, Dec. 2012.
- [12] M. A. Fischler and R. C. Bolles, "Random sample consensus: A paradigm for model fitting with applications to image analysis and automated cartography," *Commun. ACM*, vol. 24, no. 6, pp. 381–395, Jun. 1981.
- [13] R. Raguram, J.-M. Frahm, and M. Pollefeys, "A comparative analysis of RANSAC techniques leading to adaptive real-time random sample consensus," in *Proc. 10th Eur. Conf. Comput. Vis.*, 2008, pp. 500–513.
- [14] S. Mittal, S. Anand, and P. Meer, "Generalized projection-based estimator," *IEEE Trans. Pattern Anal. Mach. Intell.*, vol. 34, no. 12, pp. 2351–2364, Dec. 2012.
- [15] I. Markovsky, M. L. Rastello, A. Premoli, A. Kukush, and S. Van Huffel, "The element-wise weighted total least squares problem," *Comput. Statist. Data Anal.*, vol. 51, no. 1, pp. 181–209, Jan. 2005.
- [16] A. Kukush and S. Van Huffel, "Consistency of elementwise-weighted total least squares estimator in a multi-variate errors-in-variables model $AX = B$," *Metrika*, vol. 59, no. 1, pp. 75–97, Feb. 2004.
- [17] S. Chatterjee and M. Machler, "Robust regression: A weighted least squares approach," *Commun. Statist.-Theory Methods*, vol. 26, no. 6, pp. 1381–1394, 1997.
- [18] M. L. Rastello and A. Premoli, "Least squares problems with elementwise weighting," *Metrologia*, vol. 43, no. 4, pp. S260–S269, 2006.
- [19] M. Schuermans, I. Markovsky, and S. Van Huffel, "An adapted version of the element-wise weighted total least squares method for applications in chemometrics," *Chemometr. Intell. Lab.*, vol. 85, no. 1, pp. 40–46, Jan. 2007.
- [20] G. Plett, "Recursive approximate weighted total least squares estimation of battery cell total capacity," *J. Power Sources*, vol. 196, no. 4, pp. 2319–2331, Feb. 2011.
- [21] V. Mahboub, "On weighted total least-squares for geodetic transformations," *J. Geodesy*, vol. 86, no. 5, pp. 359–367, May. 2012.
- [22] J. R. Jensen, *Introductory Digital Image Processing: A Remote Sensing Perspective*. Englewood Cliffs, NJ, USA: Prentice-Hall, 1996.
- [23] J. A. Richards and X. P. Jia, *Remote Sensing Digital Image Analysis: An Introduction*. Berlin, Germany: Springer-Verlag, 1999.
- [24] F. H. Evans, "Statistical methods in remote sensing," in *Proc. 3rd Nat. Earth Resource Assess. Workshop*, Brisbane, QLD, Australia, 1998, pp. 1–26.
- [25] T. Wansbeek and E. Meijer, *Measurement Error and Latent Variables in Econometrics*. Amsterdam, The Netherlands: Elsevier, 2000.
- [26] P. Lancaster and M. Tismenetsky, *The Theory of Matrices With Applications*. San Diego, CA, USA: Academic, 1985.
- [27] P. M. J. Robert, "Theory and applications of weighted least squares surface matching for accurate spatial data registration," Ph.D. dissertation, School. Eng., Newcastle University, Callaghan, NSW, Australia, 2004.
- [28] Y. H. Liu, H. Zhou, X. Su, M. Ni, and R. J. Lloyd, "Transforming least squares to weighted least squares for accurate range image registration," in *Proc. 3DPVET*, 2006, pp. 232–239.
- [29] N. M. Faber and B. R. Kowalski, "Propagation of measurement errors for the validation of predictions obtained by principal component regression and partial least squares," *J. Chemometr.*, vol. 11, no. 3, pp. 181–238, May 1997.
- [30] J. W. Gillard, "An historical overview of linear regression with errors in both variables," Math. School, Cardiff Univ., Wales, U.K., Tech. Rep., 2006.
- [31] I. Markovsky, J. C. Willems, B. De Moor, and S. Van Huffel, *Exact and Approximate Modeling of Linear Systems: A Behavioral Approach*. Philadelphia, PA, USA: SIAM, 2006.
- [32] B. Schaffrin and A. Wieser, "On weighted total least squares adjustment for linear regression," *J. Geodesy*, vol. 82, no. 7, pp. 415–421, Jul. 2008.
- [33] A. Amiri-Simkooei and S. Jazaeri, "Weighted total least squares formulated by standard least squares theory," *J. Geodetic Sci.*, vol. 2, no. 2, pp. 113–124, 2012.
- [34] C. A. Glasbey and K. V. Mardia, "A review of image-warping methods," *J. Appl. Statist.*, vol. 25, no. 2, pp. 155–171, 1998.
- [35] J. J. de Guijter, D. J. Brus, M. F. P. Bierkens, and M. Knotters, *Sampling for Natural Resource Monitoring*. Berlin, Germany: Springer-Verlag, 2006.
- [36] J. H. Wang, Y. Ge, B. M. G. Heuvelink, C. H. Zhou, and D. Brus, "Effect of the sampling design of ground control points on the geometric correction of remotely sensed imagery," *Int. J. Appl. Earth Obs.*, vol. 18, no. 4, pp. 91–100, Aug. 2012.
- [37] I. Manno, *Introduction to the Monte Carlo Method*. Budapest, Hungary: Akadémiai Kiadó, 1999.
- [38] Q. X. Tong, "Beijing-1 small satellite system & its application," Beijing Land view Mapping Information Technology Co. Ltd. (BLMIIT), Beijing, China, Tech. Rep. TR-200, Feb. 10, 2011.
- [39] P. J. Huber, *Robust Statistics*. New York, NY, USA: Wiley, 1981.
- [40] P. W. Holland and R. E. Welsch, "Robust regression using iteratively reweighted least-squares," *Commun. Statist.-Theory Methods*, vol. A6, no. 9, pp. 813–827, 1977.
- [41] J. O. Street, R. J. Carroll, and D. Ruppert, "A note on computing robust regression estimates via iteratively reweighted least squares," *Amer. Statist.*, vol. 42, no. 2, pp. 152–154, 1988.



Tianjun Wu received the B.S. degree in mathematics and information science and the M.S. degree in statistics from Chang'an University, Xi'an, China, in 2009 and 2012, respectively. He is currently working toward the Ph.D. degree in cartography and geographical information system in the State Key Laboratory of Remote Sensing Sciences, Institute of Remote Sensing and Digital Earth (RAD), Chinese Academy of Sciences (CAS), Beijing, China.

In 2011, he was a Research Assistant with the State Key Laboratory of Resources and Environmental Information System, Institute of Geographical Sciences and Natural Resources Research, CAS. His research interests include remote sensing information processing and analysis, high-performance geocomputation, and statistical analysis of spatial data.



Yong Ge (M'14) received the Ph.D. degree in cartography and geographical information system from the Chinese Academy of Sciences (CAS), Beijing, China, in 2001.

She is a Professor with the State Key Laboratory of Resources and Environmental Information System, Institute of Geographical Sciences and Natural Resources Research, CAS. Her research activity focuses on spatial data analysis and data quality assessment. She has directed research in more than ten national projects. She is the author or coauthor

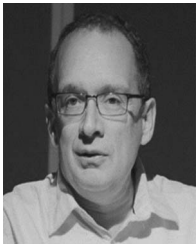
of over 80 scientific papers published in refereed journals, one book, and six chapters in books; she is the editor of one book, and she holds three granted patents in the issue of improving the accuracy of information extraction from remotely sensed imagery.

Dr. Ge has been involved in the organization of several international conferences and workshops. She is a member of the Theory and Methodology Committee of the Cartography and Geographic Information Society, the International Association of Mathematical Geosciences, and the Editorial Board of *Spatial Statistics* (Elsevier).



Jianghao Wang received the B.S. degree in geographical information system from Hohai University, Nanjing, China, in 2007 and the M.S. degree in cartography and geographical information system from the University of Chinese Academy of Sciences, Beijing, China, in 2010. He is currently working toward the Ph.D. degree in the State Key Laboratory of Resources and Environmental Information System, Institute of Geographical Sciences and Natural Resources Research, Chinese Academy of Sciences, Beijing.

His current research interests include spatiotemporal geostatistics and environmental remote sensing.



Alfred Stein received the M.Sc. degree in mathematics and information science, with a specialization in applied statistics, from the Eindhoven University of Technology, Eindhoven, The Netherlands, and the Ph.D. degree in spatial statistics from Wageningen University, Wageningen, The Netherlands.

He is a Professor of spatial statistics and image analysis with the Faculty of Geo-Information Science and Earth Observation (ITC), University of Twente, Enschede, The Netherlands. In 2000, he was appointed a Professor at the Chair of Mathematical

and Statistical Models with Wageningen University, and in 2002, he became a Professor with the new Department of Earth Observation Science, ITC, University of Twente, where he headed the department for more than ten years. In 2008, he became the Vice-Rector Research of the institute, which is a position that he had for four years. This was followed in 2012 by a position as the Portfolio Holder for Education of the management team of the faculty. Since 1998, he has been working with more than 30 Ph.D. students on a range of spatial (and temporal) statistical topics. At present, 11 Ph.D. students are working under his supervision. His research interests focus on the statistical aspects of spatial and spatiotemporal data, such as monitoring data, in the widest sense; optimal sampling; image analysis; spatial statistics; the use of prior information; but also issues of data quality, fuzzy techniques, and random sets in a Bayesian setting.

Dr. Stein is a member of the Socio-Economic and Natural Sciences of the Environment (SENSE) Research School. Since 2011, he has been the Editor-in-Chief of the *Spatial Statistics* journal, which is the new leading platform in the field of spatial statistics. It publishes articles at the highest scientific level concerning important and timely developments in the theory and applications of spatial and spatiotemporal statistics. He is an Associate Editor of the *International Journal of Applied Geoinformation and Earth Observation*.



Yongze Song received the Bachelor of Engineering in surveying and mapping engineering from the China University of Geosciences, Beijing, China, in 2012. He is currently working toward the M.S. degree in surveying and mapping science and technology at the China University of Geosciences, and is a Joint Cultivation Postgraduate in the Institute of Geographic Sciences and Natural Resources Research, Chinese Academy of Sciences, Beijing, China.

His main research interests include applying remote sensing products on geostatistics issues utilizing geographic-information-system methods or models.



Yunyan Du received the B.S. degree in cartography from Wuhan Technical University of Surveying and Mapping, Wuhan, China, in 1994 and the M.S. and Ph.D. degrees in geographic information system from the Chinese Academy of Sciences, Beijing, China, in 1997 and 2001, respectively.

She is currently an Associate Professor with the State Key Laboratory of Resource and Environmental Information System, Institute of Geographic Sciences and Natural Resources Research, Chinese Academy of Sciences. Her main research activity is in the area of remote sensing and tempo-spatial modeling. In particular, her interests are related to the interprinciple study on case-based reasoning, remote sensing information extraction, and spatial analysis. She conducts research on these topics within the frameworks of several national and international projects.

Dr. Du is a Referee for *Deep Sea Research II*, *Environment and Urban Planning*, *PLUS One*, and the *Journal of Geographical Science*. She was the recipient of the Second National Advanced Prize of Science and Technology.



Jianghong Ma received the B.S. degree in mathematics from Baoji Teachers College, Beijing, China, in 1982; the M.S. degree in applied mathematics from Northwestern Polytechnical University, Xi'an, China, in 1988; and the Ph.D. degree in applied mathematics from Xi'an Jiaotong University, Xi'an, China, in 2001.

He is currently a Professor of applied mathematics and statistics with and the Head of the Department of Mathematics and Information Science, Chang'an University, Xi'an, China. He is the author of three

textbooks on probability and statistics and of about 60 articles in professional journals and book chapters. His areas of specialization include statistical analysis, uncertainty analysis, information fusion, data mining, and pattern recognition. In particular, his interests are related to measurement error models in geographic information systems, spatial data analysis, and machine learning.

He is a Referee for the IEEE TRANSACTIONS ON NEURAL NETWORKS AND LEARNING SYSTEMS, the *International Journal of Geographical Information Science*, *Information Science*, *Science China Information Sciences*, and the *Chinese Journal of Computers*.